toxics

MDPI

Review

Recent Progress in Molecular Oxygen Activation by Iron-Based Materials: Prospects for Nano-Enabled In Situ Remediation of Organic-Contaminated Sites

Fangru He [1], Lianrui Xu [1], Hongyang Wang [2,*] and Chuanjia Jiang [1,*]

[1] College of Environmental Science and Engineering, Ministry of Education Key Laboratory of Pollution Processes and Environmental Criteria, Tianjin Key Laboratory of Environmental Remediation and Pollution Control, Nankai University, Tianjin 300350, China
[2] State Key Laboratory of Environmental Criteria and Risk Assessment, Chinese Research Academy of Environmental Sciences, Beijing 100012, China
* Correspondence: wanghongyang_why@126.com (H.W.); jiangcj@nankai.edu.cn (C.J.)

Abstract: In situ chemical oxidation (ISCO) is commonly used for the remediation of contaminated sites, and molecular oxygen (O_2) after activation by aquifer constituents and artificial remediation agents has displayed potential for efficient and selective removal of soil and groundwater contaminants via ISCO. In particular, Fe-based materials are actively investigated for O_2 activation due to their prominent catalytic performance, wide availability, and environmental compatibility. This review provides a timely overview on O_2 activation by Fe-based materials (including zero-valent iron-based materials, iron sulfides, iron (oxyhydr)oxides, and Fe-containing clay minerals) for degradation of organic pollutants. The mechanisms of O_2 activation are systematically summarized, including the electron transfer pathways, reactive oxygen species formation, and the transformation of the materials during O_2 activation, highlighting the effects of the coordination state of Fe atoms on the capability of the materials to activate O_2. In addition, the key factors influencing the O_2 activation process are analyzed, particularly the effects of organic ligands. This review deepens our understanding of the mechanisms of O_2 activation by Fe-based materials and provides further insights into the application of this process for in situ remediation of organic-contaminated sites.

Keywords: oxygen activation; Fe-based materials; reactive oxygen species; organic pollutants; groundwater contamination

check for updates

Citation: He, F.; Xu, L.; Wang, H.; Jiang, C. Recent Progress in Molecular Oxygen Activation by Iron-Based Materials: Prospects for Nano-Enabled In Situ Remediation of Organic-Contaminated Sites. *Toxics* **2024**, *12*, 773. https://doi.org/10.3390/toxics12110773

Academic Editor: Gilles Colinet

Received: 11 September 2024
Revised: 17 October 2024
Accepted: 21 October 2024
Published: 24 October 2024

1. Introduction

Groundwater is a vital resource for agricultural irrigation, drinking water supply, and industrial use. However, this valuable resource is becoming increasingly more scarce due to the excessive extraction and consumption, as well as the widely occurring groundwater pollution [1–4]. Among the various sources of groundwater contamination are closed landfills without proper maintenance and "brownfield" sites, which are abandoned lands left behind after the closure or relocation of industrial or commercial facilities [5–7]. Soil and groundwater in a majority of the sites are contaminated with various organic pollutants [8], including organic solvents (especially chlorinated solvents) [9], petroleum hydrocarbons and gasoline products (e.g., benzene, toluene, ethylbenzene, and xylenes, collectively known as BTEX) [10], polycyclic aromatic hydrocarbons (PAHs) [11,12], pesticides [13], polybrominated diphenyl ethers [14], and perfluoroalkyl and polyfluoroalkyl substances (PFASs) [15]. For example, in approximately 80% of the Superfund sites, the groundwater is contaminated with chlorinated aliphatic hydrocarbons [16]. Due to the chemical stability, low water solubility, and propensity to adsorb onto the soil medium, these organic pollutants can persist in the subsurface for many years and pose long-term environmental risks [17,18]. These organic pollutants not only cause harm to the soil and subsurface ecological environment [19,20] but also lead to adverse effects on human health [21–24]. Numerous studies have indicated that exposure to these pollutants can lead to cancer, diabetes, respiratory and neurological diseases, and reproductive disorders [25–27]. For example, exposure to PAHs accounted for a significant proportion of lung cancer cases, especially in e-waste processing areas [28]. In recent years, the toxicities and health risks of emerging organic pollutants have raised increasing attention. Notably, PFASs can cause immunotoxicity, cardiotoxicity, and pancreatic and liver damage, as well as endocrine-disrupting effects [29,30]. Therefore, it is urgent to formulate effective strategies for mitigating the ecological and health risks posed by these legacy and emerging organic pollutants.

Intensive studies have been conducted to develop remediation technologies for soil and groundwater with organic contamination [31–33]. Among the various remediation technologies, in situ chemical oxidation (ISCO) methods have received increasing attention due to their high efficiency and simple operation [34–36]. During ISCO processes, oxidants such as ozone, potassium permanganate, hydrogen peroxide (H_2O_2), and persulfate are injected into the contaminated source zone and then activated when needed, generating stronger oxidizing species, such as hydroxyl radical (•OH) and sulfate radical [34,36,37]. However, these commonly used oxidants still suffer from some drawbacks, such as low selectivity, rapid consumption by aquifer constituents, and the risk of secondary pollution. In particular, their efficiency and cost-effectiveness for removing residual non-aqueous phase liquids (NAPL) pollutants is low.

Recent studies have found that molecular oxygen (O_2) is an ideal green alternative to the traditional oxidants for ISCO remediation of contaminated soil/sediment and groundwater. O_2 is relatively stable due to unfavorable one-electron reduction chemistry and spin restriction [38], which is favorable for its delivery to the pollutants without extensive consumption by aquifer constituents during its transport in the subsurface porous media. Additionally, groundwater table fluctuation, which can be caused by evaporation and rainfall, tide, lateral recharge, and drainage, results in the trapping of O_2 in unsaturated soil and saturated aquifers [39]. Under certain conditions, O_2 could be activated to form reactive oxygen species (ROS), such as •OH, singlet oxygen ($^1O_2$) and superoxide radical ($O_2^{\bullet-}$), and H_2O_2 [40], mainly via electrochemical- [41], photochemical- [42], and chemical-activation approaches [38]. The electrochemical- and photochemical-activation methods require electrical power and light irradiation, as well as devices that may not be facilely emplaced underground, which greatly hinders the application of these methods for in situ remediation of contaminated sites. In contrast, the chemical activation of O_2 by earth-abundant elements holds great promise for in situ soil and groundwater remediation.

Iron is the fourth-most-abundant element in the Earth's crust, and Fe-containing minerals are ubiquitous in soils and aquifers [43–45]. Iron-based materials are extensively investigated for applications in environmental remediation, exhibiting high efficiency in degrading a range of organic pollutants (Table 1) due to the redox and catalytic activities of the Fe element and the versatility, availability, and environmental compatibility of Fe-based materials [46,47]. For example, zero-valent iron (ZVI)-based materials are the most widely used agents for in situ chemical-reduction remediation [48–53]. Meanwhile, Fe-based materials can promote ISCO remediation by the activation of H_2O_2/CaO_2 [54–58], persulfates [59–63], and other oxidants [64–66]. Moreover, Fe-based materials such as ZVI [67,68], iron sulfides [69,70], iron (oxyhydr)oxides [71], and Fe-containing clay minerals [72] can mediate O_2 activation to degrade organic pollutants, and the potential of Fe-mediated O_2 activation for ISCO remediation has been actively explored in recent years. However, there is a lack of a timely review of the mechanisms and key influencing factors of O_2 activation by iron-based materials for potential applications for in situ remediation of soil- and groundwater-suffering organic contamination.

Table 1. Degradation of organic pollutants by Fe-based materials via different mechanisms.

Pollutant	Material	Reaction Mechanism	Reference
Trichloroethylene	nZVI	Reductive dechlorination	[48]
Trichloroethylene	mZVI	Reductive dechlorination	[49]
Trichloroethylene	S-nZVI	Reductive dechlorination	[50]
Trichloroethylene	S-mZVI	Reductive dechlorination	[49]
Trichloroethylene	Fe_xN	Reductive dechlorination	[51]
Chloroform	S–N(C)–ZVI	Reductive dechlorination	[52]
Florfenicol	S-nZVI	Reductive dehalogenation	[53]
Fluorenone	Fe_3O_4	H_2O_2 activation	[54]
Trichloroethylene	Reduced nontronite	H_2O_2 activation	[55]
Diethyl phthalate	Reduced nontronite	H_2O_2 activation	[56]
Trichloroethylene	FeS	CaO_2 activation	[57]
Sulfanilamide	FeS_2	CaO_2 activation	[58]
Phenanthrene	FeCo-BDC	Peroxymonosulfate activation	[59]
Perfluorooctanic acid	Fe/AC	Persulfate activation	[60]
Trichloroethylene	nZVI	Persulfate activation	[61]
Ciprofloxacin	FeS_2	Persulfate activation	[62]
Bisphenol A	Fe_3S_4	Peroxymonosulfate activation	[63]
Bisphenol AF	FeS	Periodate activation	[64]
Tetracycline	ZVI	Peracetic acid activation	[65]
Sulfamethoxazole	FeS	Peracetic acid activation	[66]

Note: ZVI, zero-valent iron; nZVI, nanoscale ZVI; mZVI, microscale ZVI; S-nZVI, sulfidated nZVI; S-mZVI, sulfidated mZVI; Fe_xN, iron nitrides; S–N(C)–ZVI, ZVI treated by nitridation and sulfidation; BDC, bimetallic metal-organic frameworks; AC, activated carbon.

Herein, we comprehensively review the current status of research on the activation of O_2 by Fe-based materials, including ZVI-based materials, iron sulfides, iron (oxyhydr)oxides, and Fe-containing clay minerals for degrading contaminants commonly found in soil/sediment and groundwater. Unlike previous reviews on O_2 activation, which highlight more efficient techniques such as electrochemical and photochemical activation for rapid abatement of pollutants (e.g., in wastewater treatment) [73–76], this review focuses on O_2 activation by Fe-based materials without external energy input, which holds better promise for application in the remediation of organic-contaminated sites. Particularly, this review includes discussions on recent research in O_2 activation by reduced Fe-bearing minerals abundant in soils and sediments, which has important implications for slower but sustained remediation via natural attenuation processes. The major mechanisms involved in the activation of O_2 by the Fe-based materials are summarized, highlighting electron transfer and utilization, reaction intermediates and ROS chain reactions, and the oxidative transformation of the materials during the O_2-activation process are discussed. Additionally, we discussed the influences of environmental and operational factors, including O_2 concentration, organic ligands, inorganic anions, and microbial activity, on the O_2 activation and pollutant-degradation performance by iron-based materials. This review also identifies limitations of current studies and suggests future research directions to enhance understanding of O_2 activation by iron-based materials and its applications in soil and groundwater remediation.

2. Activation of O_2 by Fe-Based Materials

2.1. ZVI-Based Materials

Materials containing ZVI have been commonly employed as remediation agents for reductive degradation of organic pollutants under anaerobic conditions due to the high reducing capacity of elemental Fe (Table 2) [77–83]. However, studies have indicated that the degradation efficiency of organic pollutants by ZVI is significantly higher in O_2-containing aqueous solutions than under anaerobic conditions [67,84,85], and O_2 activation by ZVI-based materials has recently been extensively explored for degrading various organic pollutants (Table 3). This increased efficiency is primarily attributed to the reaction between ZVI and O_2, which leads to the generation of ROS [67,68]. The mechanism of ZVI-mediated O_2 activation for the generation of ROS involves two-electron transfers from Fe^0 to adsorbed O_2, producing Fe(II) and H_2O_2. And the release of Fe(II) further induces O_2 activation via a sequential single-electron transfer process, generating •OH, $O_2^{\bullet-}$, and other ROS (Equations (1)–(6)) [86]. The yield of •OH is primarily affected by the reaction between Fe^0 and O_2 via four-electron transfer without ROS generation (Equation (7)) [87]. Due to this reaction pathway, only less than 10% of the ZVI is utilized for contaminant transformation under oxic conditions [88]. Therefore, the yield of ROS decreases with increasing pH due to the inhibition of Fe(II) release via the four-electron-transfer reaction under high pH conditions [84]. Notably, the ROS generation is influenced by the oxide layer on the surface of ZVI, in a fashion dependent on the thickness of the layer [89]. The iron oxide layer can adsorb ferrous ions, which can activate O_2 through a single-electron-transfer pathway. When the iron oxide layer is thin, both the Fe^0 core-mediated two-electron transfer and the surface-bound/adsorbed Fe(II)-mediated single-electron transfer play significant roles in O_2 activation [73]. However, as the thickness of the oxide layer increases, it inhibits electron transfers from the Fe^0 core to adsorbed O_2. Meanwhile, more ferrous ions are adsorbed on the surface, and these surface-bound Fe(II) become the primary species responsible for O_2 activation (Figure 1a) [75,89,90].

$$Fe^0 + O_2 + 2H^+ \rightarrow Fe(II) + H_2O_2 \tag{1}$$

$$Fe(II) + O_2 \rightarrow Fe(III) + O_2^{\bullet-} \tag{2}$$

$$Fe(II) + O_2^{\bullet-} + 2H^+ \rightarrow Fe(III) + H_2O_2 \tag{3}$$

$$O_2^{\bullet-} + H^+ \rightarrow HO_2^{\bullet} \tag{4}$$

$$HO_2^{\bullet} + HO_2^{\bullet} \rightarrow H_2O_2 + O_2 \tag{5}$$

$$Fe(II) + H_2O_2 \rightarrow Fe(III) + \bullet OH + OH^- \text{ or } Fe(IV) + 2OH^- \tag{6}$$

$$2Fe^0 + O_2 + 4H^+ \rightarrow 2Fe(II) + 2H_2O \tag{7}$$

Table 2. Redox potential of different Fe species.

Species	Redox Potential (V)	Reference
Fe^0/Fe(II)	−0.44 (vs. SHE)	[80]
Structural Fe(II)/Fe(III) of pyrite	0.66 (vs. SHE)	[81]
Structural Fe(II)/Fe(III) of clay mineral	−0.6 to +0.6 (vs. SHE)	[82]
Fe(III)/Fe(II)-CA	0.37 (vs. NHE)	[83]
Fe(III)/Fe(II)-OA	0.002 (vs. NHE)	[83]
Fe(III)/Fe(II)-EDTA	0.12, 0.11, and 0.096 (vs. NHE)	[83]
Fe(III)/Fe(II)-EDDS	0.19 (vs. NHE)	[83]
Fe(III)/Fe(II)-NTA	0.10 and 0.39 (vs. NHE)	[83]
$Fe(H_2O)_6^{2+}/Fe(H_2O)_6^{3+}$	0.77 (vs. NHE)	[83]

Note: SHE, standard hydrogen electrode; NHE, normal hydrogen electrode; CA, citrate; OA, oxalate; EDTA, ethylenediaminetetraacetic acid; EDDS, N,N′-1,2-ethanediylbis-1-aspartic acid; NTA, nitilotriacetic acid.

Table 3. Degradation of organic pollutants via O_2 activation by ZVI-based materials.

Material	Pollutant	Removal Ratio (%)	Reaction Time (h)	pH	Rate Constant	Reference
ZVI	EDTA	100	2.5	6.0 ± 0.2	1.02 h^{-1}	[68]
nZVI	2-Chlorobiphenyl	59.4	4	5.0	0.0035 min^{-1}	[84]
S-nZVI	Bisphenol A	100	6	5.0	59.2 ± 2.29 h^{-1}	[85]
$Fe@Fe_2O_3$	4-Chlorophenol	77.8	7	6.0	0.22 h^{-1}	[89]
Al–Fe	4-Chlorophenol	43.7	5	2.5	N/A	[91]
Fe/Cu	4-Chlorophenol	100	2	3.0	N/A	[92]
Fe/Cu	Diclofenac	96	2	6.0	N/A	[93]
Mg/Fe	4-Chlorophenol	100	0.75	3.0	N/A	[94]

Table 3. *Cont.*

Material	Pollutant	Removal Ratio (%)	Reaction Time (h)	pH	Rate Constant	Reference
Fe/Mn	Enrofloxacin	100	1	3.0	N/A	[95]
ZVI	Enrofloxacin	58.6	1	3.0	N/A	[95]
S-nZVI	p-Nitrophenol	99.3 *	2	7.6	$0.769\ min^{-1}$	[96]
mZVI/NGB	Tetracycline	100	0.83	5.8	N/A	[97]
3D-GN@nZVI	Sulfadiazine	81.0	2	3.0	N/A	[98]
Cu/Fe-BC	Ciprofloxacin	93.2 *	1.5	5.0	$0.052\ min^{-1}$	[99]
Cu/Fe-BC	Enrofloxacin	88.9 *	1.5	5.0	$0.036\ min^{-1}$	[99]
Cu/Fe-BC	Norfloxacin	95.4 *	1.5	5.0	$0.096\ min^{-1}$	[99]
Cu/Fe-BC	Tetracycline	82.3 *	1.5	5.0	$0.037\ min^{-1}$	[99]
Cu/Fe-BC	Methylene blue	95.6 *	1.5	5.0	$0.145\ min^{-1}$	[99]
ZVI-BC	Tetracycline	93.1	6	Unadjusted	N/A	[100]
Zn-Fe-CNTs	Sulfamethoxazole	95.3	0.33	1.5	N/A	[101]
Zn-Fe-CNTs	4-Chlorophenol	90.8	0.33	2.0	N/A	[102]
nZVI@MSN	Nitrobenzene	96.5	0.33	3.0	$0.201\ min^{-1}$	[103]

Note: N/A, data not available. *, data obtained from the literature using the Getdata 2.26 software.

To improve the O_2-activation efficiency and ROS yield, various modified ZVI materials have been developed, notably by doping with metal and non-metal elements or immobilizing ZVI on porous materials. Inspired by the galvanic corrosion between connected dissimilar metals [91], a series of ZVI-based bimetallic materials were designed. In a Cu^0/ZVI material, Cu^0 can enhance the reaction potential by forming infinite galvanic cells with Fe^0, thereby significantly accelerating Fe-mediated O_2 activation [92]. Additionally, Cu accelerates the release of Fe(II) species during O_2 activation (Figure 1b). Furthermore, Cu species can also effectively facilitate the iron cycle and serve as new active sites (Equations (8)–(12)) [93]. However, it has also been suggested that Cu may inhibit •OH generation due to the formation of a passivation layer of Cu oxides [104]. This discrepancy may be attributed to the complex chain reactions and the dosage of Cu, which should earn more attention in further studies. Another metal element, Ni, has been shown to reduce the proportion of the four-electron-reaction pathway of ZVI by increasing Fe(II) release [88]. Alternatively, the Fe–Mg bimetallic material can increase the degradation of 4-chlorophenol by enhancing the generation of surface-bound •OH [94]. Recently, a Fe–Mn core-shell bimetallic material was reported for O_2 activation and on-site generation of H_2O_2, and it was proposed that the amorphous Mn shell can not only protect the Fe core from excessive oxidation, thereby increasing electron utilization, but also contain abundant structural defects, which serve as efficient catalytic sites [95]. Doping with non-metal elements can also affect the efficiency of O_2 activation by ZVI materials. For example, the incorporation of chloride ions into microscale zero-valent iron (mZVI) can create oxygen vacancies (OVs), resulting in abundant adsorbed ferrous ions and accelerated electron transfer [105]. Sulfidation is one of the most effective methods to improve the efficiency and selectivity of reductive degradation of pollutants by nanoscale ZVI (nZVI) [106–109], and it has been demonstrated that the presence of S could enhance electron transfers from the Fe^0 core to surface Fe(III) and O_2 via the single-electron pathway, thus promoting pollutant degradation under aerobic conditions [96,110].

$$Cu^0 + Fe(III) \rightarrow Cu(I) + Fe(II) \quad (8)$$

$$Cu(I) + Fe(III) \rightarrow Cu(II) + Fe(II) \quad (9)$$

$$Cu^0 + O_2 + 2H^+ \rightarrow Cu(II) + H_2O_2 \quad (10)$$

$$Cu(I) + O_2 \rightarrow Cu(II) + O_2^{\bullet -} \quad (11)$$

$$Cu(I) + O_2^{\bullet -} + 2H^+ \rightarrow Cu(II) + H_2O_2 \quad (12)$$

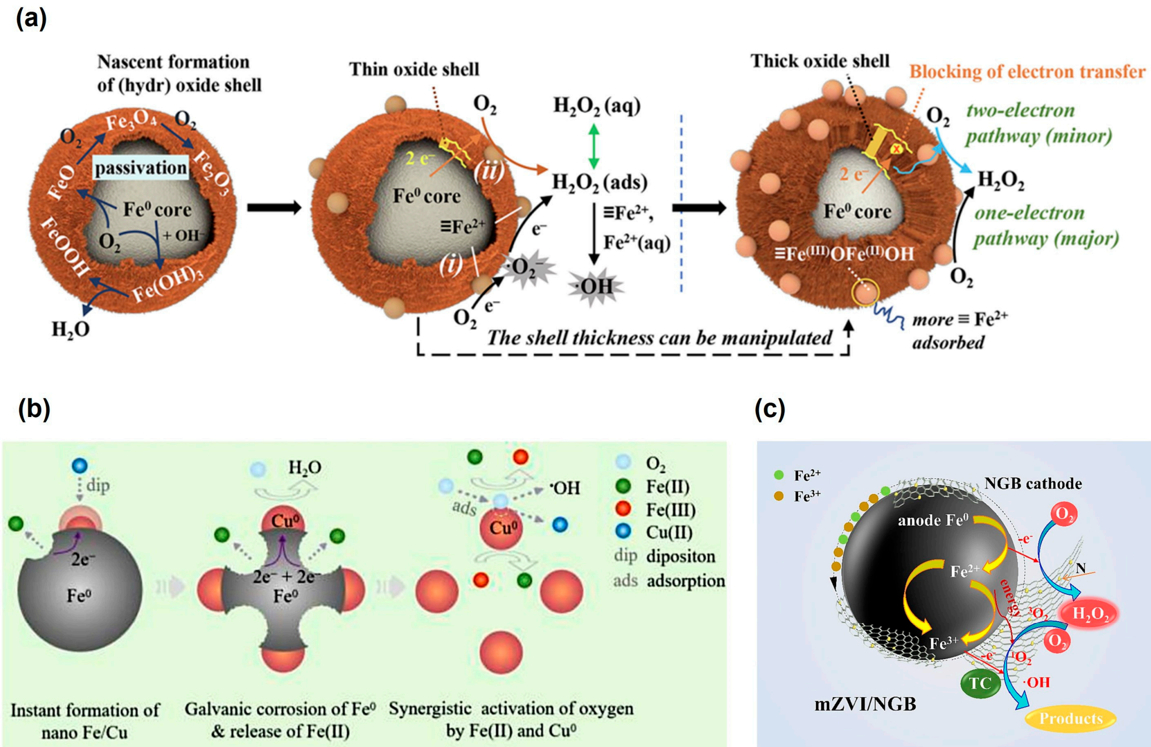

Figure 1. (**a**) Illustration of the mechanisms of O_2 activation by Fe^0 with an oxide shell of different thickness [73]. (**b**) Illustration of the mechanisms of Cu-enhanced •OH production in Cu^0/ZVI system under oxic condition [93]. (**c**) Illustration of the catalytic mechanism of O_2 by mZVI/N-doped graphene-like biochar (mZVI/NGB) [97].

Another approach to enhancing ZVI performance involves immobilizing ZVI on porous supports, particularly carbon materials. The carbon materials (e.g., graphene), usually with a conjugated network skeleton of sp^2 hybridized carbon atoms, could enhance electron transfer and modify the adsorption/dissociation energy of O_2, making O_2 activation thermodynamically and kinetically more favorable [111–113]. Meanwhile, the combination of ZVI with graphene (3D-GN@nZVI) can also greatly inhibit the reduction of O_2 to H_2O via a four-electron process, thereby increasing the yield of ROS [98]. Recent studies have indicated that a mZVI/N-doped graphene-like biochar composite (mZVI/NGB) could promote the contribution of non-radical pathways ($^1O_2$ and electron transfer) during O_2 activation for antibiotics degradation (Figure 1c) [97]. Similarly, for Fe/Cu-biochar (Cu/Fe-BC) materials, both radicals (e.g., $O_2^{\bullet-}$, •OH) and non-radicals (e.g., $^1O_2$) were detected as the dominant reactive species, enabling the efficient degradation of a wide spectrum of organic pollutants, even in the presence of various interfering substances [99]. In contrast, $O_2^{\bullet-}$ and H_2O_2 are the key ROS in the ZVI–biochar system, indicating that the secondary metal has a significant influence on the O_2-activation pathway [100]. Carbon nanotubes (CNTs) have also been demonstrated as an excellent support material to regulate ROS generation dynamics by bimetallic Fe-based materials. For example, in a Zn–Fe–CNT composite, CNTs effectively collect electrons from Zn^0 nanoparticles and reduce O_2 to H_2O_2, which was subsequently converted to •OH by Fe^0 nanoparticles [101,102]. Due to the synergistic effects, the composite achieved excellent performance for the degradation of 4-chlorophenol and sulfamethoxazole (Table 3). In addition to carbon materials, nZVI can also be successfully incorporated within the channels of monodisperse mesoporous silica nanospheres (nZVI@MSN) to increase its stability and durability [103].

2.2. Iron Sulfides

2.2.1. Pyrite

Pyrite (FeS_2) is the most widely distributed stable-phase iron sulfide mineral in Earth's crust [114]. The oxidation of natural pyrite, which can lead to the generation of H_2O_2, has been confirmed under anaerobic conditions [115]. The mechanism involved in this process is primarily attributed to the presence of surface defects, arising from the cleavage of the S–S bond [116]. As a result, transient S– and ≡Fe(III) dangling bonds are generated at these sulfur-deficient defect sites, which can induce the formation of •OH by extracting an electron from adsorbed H_2O, and the •OH radicals then combine to form H_2O_2 in the absence of O_2 [117]. In a recent study investigating oxidation of benzoic acid by sulfur vacancy (SV)-rich FeS_2 in isotopically labeled $H_2{}^{18}O$, the generation of ^{18}O-containing *p*-hydroxybenzoic acid was observed, which further provided direct evidence that the anaerobic oxidation of water by SV-rich FeS_2 is responsible for the generation of •OH at the pyrite–water interface [118]. However, it was noted that the •OH generated through this mechanism was insufficient to achieve an obvious degradation of organic pollutants. In contrast, efficient pollutant removal can be achieved in pyrite suspension with sufficient O_2 (Table 4), which highlights the crucial role of pyrite oxidation by O_2 [70,119].

Table 4. Degradation of organic pollutants via O_2 activation by iron sulfides.

Material	Pollutant	Removal Ratio (%)	Reaction Time (h)	pH	Rate Constant	Reference
Pyrite	Trichloroethylene	100	323	4.0	$0.013\ h^{-1}$	[70]
Pyrite	Acid orange 7	52.8	5	6.3	N/A	[120]
Pyrite	Carbamazepine	81.5	24	7.0	$0.103 \pm 0.001\ h^{-1}$	[121]
Pyrite	Phenol	76.8	24	7.0	$0.084 \pm 0.001\ h^{-1}$	[121]
Pyrite	Bisphenol A	100	24	7.0	$0.147 \pm 0.001\ h^{-1}$	[121]
SV-rich pyrite	Sulfamethoxazole	88.3	12	8.5	$29.2 \times 10^{-4}\ h^{-1}$	[122]
Pyrite	Sulfamethoxazole	70.0	12	4.0	$0.095\ h^{-1}$	[123]
Mackinawite	Flumequine	79.8	4	7.0	$51.6 \times 10^{-3}\ min^{-1}$	[124]
Mackinawite	Enrofloxacin	87.7	4	7.0	$34.0 \times 10^{-3}\ min^{-1}$	[124]
Mackinawite	Ciprofloxacin	81.5	4	7.0	$25.4 \times 10^{-3}\ min^{-1}$	[124]
Mackinawite	Trichloroethylene	23.4 *	3	7.0	$2.07 \times 10^{-3}\ min^{-1}$	[69]
Mackinawite	Phenol	34.1 *	3	7.0	$3.53 \times 10^{-3}\ min^{-1}$	[69]
Surface-oxidized mackinawite	Phenol	17.5 *	1.5	7.3	$3.8 \times 10^{-3}\ min^{-1}$	[125]

Note: N/A, data not available. SV, sulfur vacancy. *, data obtained from the literature using the Getdata 2.26 software.

The mechanism for O_2 activation by pyrite can be understood from an analysis of the Fe species in pyrite suspension (Equations (13)–(18)). Previous studies have proposed that structural Fe(II) and surface-bound Fe(II) can mediate either a two-electron-transfer pathway or two separate one-electron-transfer processes, with H_2O_2 or $O_2{}^{\bullet-}$ as intermediates, ultimately leading to the formation of •OH (Figure 2a) [119,126]. Another pathway involves the leaching of dissolved Fe(II) from bulk FeS_2, which mediates O_2 activation in aqueous solution via a single-electron-transfer pathway [127]. However, the contribution of this approach is generally minor due to the stable structure and extremely low dissolution rate of pyrite even under acidic conditions [120,128]. Moreover, the reactivity of dissolved Fe(II) is lower than the structural Fe(II) and surface-bound Fe(II) according to their redox potentials (Table 2) [72,129]. Note that, although $S_2{}^{2-}$ has the capability to reduce surface-bound Fe(III), it does not directly participate in O_2 reduction [130]. This inference is substantiated by the results of in situ horizontal attenuated total reflectance infrared spectroscopy and isotope analysis of reaction products (e.g., $SO_4{}^{2-}$ and iron oxyhydroxide), which demonstrated that the O atoms in $SO_4{}^{2-}$ primarily originate from H_2O, while the O atoms in the iron oxyhydroxide are derived from O_2 [131,132].

$$\equiv Fe(II) + O_2 + 2H^+ \rightarrow Fe(III) + H_2O_2 \tag{13}$$

$$Fe(II)_{ad} + O_2 \rightarrow Fe(III) + O_2^{\bullet-} \tag{14}$$

$$Fe(II) + O_2^{\bullet-} + 2H^+ \rightarrow Fe(III) + H_2O_2 \tag{15}$$

$$Fe(II)_{(aq)} + O_2 \rightarrow Fe(III)_{(aq)} + O_2^{\bullet-} \tag{16}$$

$$Fe(II)_{(aq)} + O_2^{\bullet-} + 2H^+ \rightarrow Fe(III)_{(aq)} + H_2O_2 \tag{17}$$

$$H_2O_2 + Fe(II) \rightarrow Fe(III) + \bullet OH + OH^- \tag{18}$$

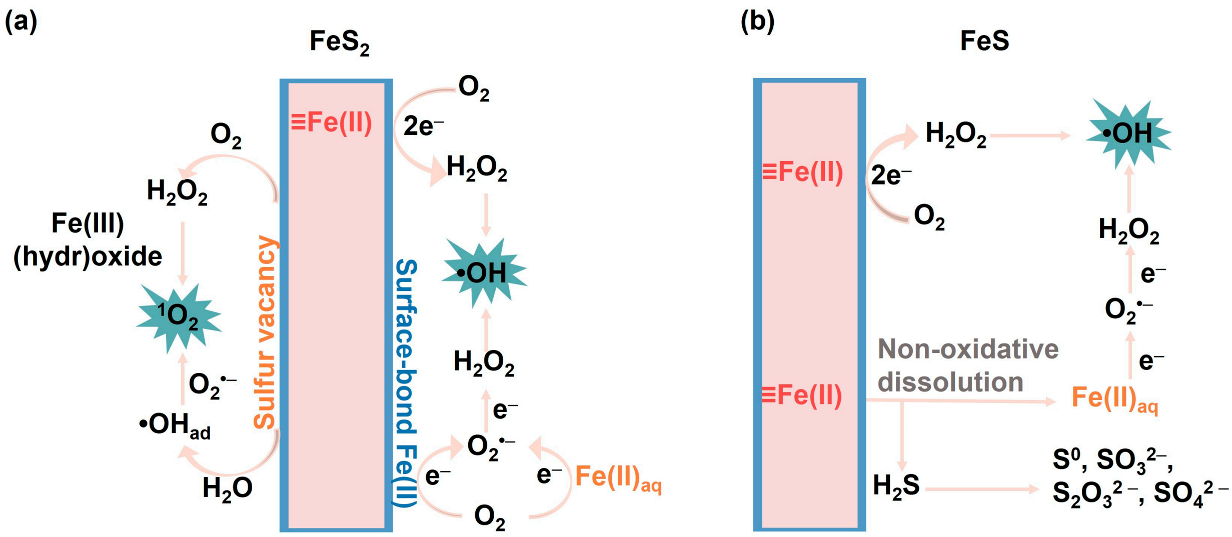

Figure 2. Illustration of the mechanisms of O_2 activation by (**a**) FeS_2 and (**b**) FeS.

As an interfacial reaction, the efficiency of O_2 activation by pyrite is dictated by the surface properties of pyrite, which in turn is dependent on the exposed facets, the presence of surface defects, and the formation of the iron (oxyhydr)oxide layer. The exposed facets of pyrite significantly influence the O_2-activation configurations and electron-transfer ability [133]. Notably, it has been recently revealed that pyrite crystals with more exposed {210} facets exhibit higher generation rates of •OH and other ROS (e.g., $O_2^{\bullet-}$ and H_2O_2) due to different surface electron-donating capacities and kinetics among different facets. Correspondingly, facet-dependent degradation of organic pollutants (e.g., carbamazepine, phenol, and bisphenol A) was achieved [121]. Another recent study highlighted that SV sites in pyrite can activate O_2 via a two-electron-transfer mechanism, generating $^1O_2$, which played a key role in the selective degradation of sulfamethoxazole [122]. The generation of $^1O_2$ arises from the breakage of the O–H bond in H_2O_2, facilitated by Fe(III) (oxyhydr)oxide on the pyrite surface, as presented by Equations (19) and (20) [122], whereas another recent study proposed that $^1O_2$ could also form through the interaction between surface-bound •OH and $O_2^{\bullet-}$ in the pyrite-oxidation process (Equations (21) and (22)) [123]. The iron (oxyhydr)oxides on the surface of pyrite, which quickly forms after pyrite is exposed to O_2, can also affect ROS generation during O_2 activation in the pyrite system in both positive and negative ways. The formation of iron (oxyhydr)oxides can provide fast electron-transfer channels by establishing a potential gradient between the two mineral phases [134]. Additionally, the iron (oxyhydr)oxides can adsorb more surface-bound Fe(II) by forming inner-sphere complexes with surface groups, thereby enhancing O_2-reduction efficiency [135]. However, other studies indicated that the (oxyhydr)oxide coating tends to lower the H_2O_2 utilization by catalyzing its transformation into H_2O, resulting in the decrease of ROS concentration in the system [136–138].

$$Fe(III)_{(SV\text{-}Pyrite)} + O_2 \rightarrow H_2O_2 \tag{19}$$

$$H_2O_2 \rightarrow {}^1O_2 + 2H^+ \tag{20}$$

$$Fe(III)_{(SV\text{-}Pyrite)} + H_2O \rightarrow Fe(II)_{(SV\text{-}Pyrite)} + \bullet OH_{ad} + H^+ \quad (21)$$

$$O_2^{\bullet-} + \bullet OH_{ad} \rightarrow {}^1O_2 + OH^- \quad (22)$$

2.2.2. Mackinawite

Mackinawite (FeS) is a metastable iron sulfide mineral, which can readily convert into more stable phases, such as FeS_2 and greigite (Fe_3S_4) in a natural environment [139]. Due to its structural instability and reducing power, FeS is prone to oxidation by O_2, and oxidative transformation of pollutants (e.g., As(III) and U(IV)) has been observed during FeS oxidation under aerobic conditions, and different oxidative species (e.g., •OH, Fe(IV), and transient surface Fe(III) species) have been proposed to initiate the pollutant degradation [140–142]. Yuan's group confirmed the production of •OH during the oxidation of FeS by O_2 and demonstrated that the produced •OH played a key role in the oxidation of As(III) [143]. The rate of •OH formation by mackinawite is one-to-two orders of magnitude higher than that observed for other forms of reduced iron minerals, such as nontronite, pyrite, and siderite ($FeCO_3$), under comparable conditions due to the metastable structure and higher Fe(II) content [143,144]. The ROS produced during FeS oxidation can also efficiently degrade various organic pollutants, such as phenol, trichloroethylene (TCE), and fluoroquinolone antibiotics [69,124].

The mechanism of FeS oxidation by O_2 is dependent on the pH conditions. When pH is lower than 3, FeS primarily undergoes non-oxidative dissolution, and most of the structural Fe(II) in FeS enters the aqueous solution before undergoing oxidation, which leads to an increase in dissolved ferrous ion concentration and the generation of H_2S (Equation (23)) (Figure 2b) [140,145]. The dissolved ferrous ions can mediate homogeneous Fenton processes [127]. Surface-mediated oxidative dissolution also occurs under acidic conditions, due to the formation of an iron (oxyhydr)oxide layer, which can adsorb Fe(II) on the surface, activating O_2 to form ROS [135]. Under neutral pH conditions, due to the low concentration of dissolved iron ions, surface-mediated oxidation mechanisms predominate, with surface species of FeS transforming from ≡Fe(II)–S through ≡Fe(III)–S to ≡Fe(III)–O in the presence of O_2 [140]. This structural Fe(II)-mediated heterogeneous reaction dominates the O_2 activation and ROS production reactions in the FeS system under neutral conditions [143], which involves a two-electron-transfer mechanism, leading to the generation of H_2O_2 intermediate and subsequent formation of •OH [143,146]. Notably, in addition to aqueous •OH, other active species such as high-valent iron, surface-bound •OH, or sulfur-based radicals may also be present in the FeS/O_2 system [147]. Apart from structural Fe(II), S(–II) can also act as the electron donator, mediating the iron cycle without directly participating in the O_2-activation process [143]. As with FeS_2, the Fe (oxyhydr)oxide coatings formed on the surface of FeS could affect O_2-activation efficiency by mediating electron transfers from FeS to O_2. Interestingly, the storage of partially oxidized FeS under anoxic conditions could change its mineralogical structure and surface Fe speciation, forming new Fe(II) species in the (oxyhydr)oxide layer, which leads to enhanced reactivity toward O_2 and the production of ROS [125].

$$FeS + 2H^+ \rightarrow Fe(II)_{(aq)} + H_2S_{(aq)} \quad (23)$$

2.3. Iron (Oxyhydr)Oxides

Magnetite (Fe_3O_4) is one of the most widely distributed reductive iron oxides in the subsurface environment, and it can activate O_2 to generate $O_2^{\bullet-}$, H_2O_2, and •OH and has been used for organic pollutant degradation (Table 5) [71,148,149]. Structural Fe(II) is considered the dominant species participating in O_2 activation in magnetite via a single-electron transfer under alkaline conditions, whereas dissolved iron ions originating from the dissolution of magnetite can participate in O_2 activation at pH < 6.5 [71]. Interior structural iron could facilitate O_2 activation by transferring electrons to surface iron and accelerating the iron cycle [150]. Nevertheless, studies have indicated that only half of the total Fe(II) in magnetite could be effectively utilized due to the low inner-electron-transfer ability, leading to a low O_2-activation efficiency [71]. Notably, it has been proposed that the presence of OVs can change the Gibbs free energy for the generation of adsorbed O_2 intermediate, making the reduction of O_2 thermodynamically more favorable and facilitating the electron transfer [148].

Table 5. Degradation of organic pollutants via O_2 activation by iron (oxyhydr)oxides.

Material	Pollutant	Removal Ratio (%)	Reaction Time (h)	pH	Rate Constant	Reference
Magnetite	2-Chlorobiphenyl	80	4	3.0	N/A	[149]
Cu^0/Fe_3O_4	4-Chlorophenol	99.5	1	7.0	0.073 min^{-1}	[151]
Zn^0-CNTs-Fe_3O_4	4-Chlorophenol	99	0.33	1.5	N/A	[152]
CNTs-Fe_3O_4	4-Chlorophenol	25	0.33	1.5	N/A	[152]
b-CoS_2/Fe_3O_4	4-Nitrophenol	62.3 *	0.25	5.0	N/A	[153]
b-CoS_2/Fe_3O_4	Methyl orange	85.7	0.25	5.0	N/A	[153]
b-CoS_2/Fe_3O_4	Sulfadiazine	67.1	0.25	5.0	N/A	[153]
b-CoS_2/Fe_3O_4	Tetracycline	96.0	0.25	5.0	N/A	[153]
b-CoS_2/Fe_3O_4	Rhodamine b	98.6 *	0.25	5.0	N/A	[153]
b-CoS_2/Fe_3O_4	Malachite green	91.5 *	0.25	5.0	N/A	[153]
Ferrihydrite	Phenol	29.8 *	10	7.0	N/A	[154]

Note: N/A, data not available. *, data obtained from the literature using the Getdata 2.26 software.

To improve the efficiency of O_2 activation, many synthetic Fe_3O_4-based composite materials have also been designed. For example, in a carboxylated Cu^0/Fe_3O_4 system, Cu^0 can act as the reducing agent and accelerate the regeneration of surface iron. In addition, Cu^0 serves as a new O_2 activation site to further increase the generation of H_2O_2 in the system via two-electron transfer, leading to the efficient removal of chlorophenol [151]. Similarly, Fe_3O_4 can mediate the ROS-generation dynamics of carbon-supported zero-valent metal, thus increasing the overall O_2-activation efficiency. For example, in a Zn^0–CNT–Fe_3O_4 composite, with Zn^0 and Fe_3O_4 nanoparticles well dispersed on the surface of CNTs, the self-decomposition of H_2O_2 (generated from O_2 reduction by Zn^0 on CNTs surface) into H_2O is significantly inhibited. Meanwhile, the conversion of H_2O_2 into •OH rapidly occurs with a high yield [152]. As a result, the Zn^0–CNT–Fe_3O_4 composite exhibited approximately four times higher removal efficiency for 4-chlorophenol than that by CNT-Fe_3O_4 and Zn^0–CNT materials [152]. Moreover, sulfidation can lead to higher H_2O_2 and •OH production during Fe_3O_4 oxidation because surface sulfur species can decrease electron-transfer resistances of Fe_3O_4, thereby accelerating the electron transfer from interior structural iron to the surface Fe(III) and facilitating the reaction between surface iron and O_2 [155]. Moreover, for a vacancy-rich iron-cobalt bimetallic composite prepared by ball milling CoS_2 and Fe_3O_4 (b-CoS_2/Fe_3O_4), the interfacial interaction between CoS_2 and Fe_3O_4 can change the Fe–O bond energy of Fe_3O_4, thereby accelerating the formation of surface-bound Fe(II), which in turn promotes O_2 activation by the composite [153].

Fe(III) (oxyhydr)oxides such as goethite (α-FeOOH) and hematite (α-Fe_2O_3) generally lack the ability to reduce O_2 due to the +3 valence state of iron in these compounds. However, studies have indicated that Fe(III) (oxyhydr)oxides can adsorb Fe(II) on their surface, and these surface-bound Fe(II) can activate O_2 through a single-electron-transfer process [156,157]. Furthermore, the incorporation of Cu into goethite can increase the O_2-activation ability of surface-bound Fe(II) by modifying the adsorption energy of O_2, lowering its oxidation potential, and increasing the interfacial electron-transfer process on Fe(III) (oxyhydr)oxides [156]. The incorporation of secondary metal atoms can also increase the content of OVs in hematite, further enhancing the electron-transfer efficiency [150]. Notably, the incorporation of secondary metals does not necessarily have a positive effect on the O_2-activation efficiency. For example, the incorporation of Zn results in a higher oxidation potential for Fe(II) oxidation, which is unfavorable for the O_2-activation process [150]. Moreover, it was recently proposed that Fe(III) (oxyhydr)oxides can serve as an electron-transfer mediator for O_2 reduction by reducing organic compounds to generate ROS. Specifically, Fe(III) on their surface receives electrons from the reducing organic compounds, such as thiols, to form surface Fe(II), which then mediate the activation of O_2 efficiently [154].

2.4. Fe(II)-Containing Clay Minerals

Fe(II)-containing clay minerals are widely present in subsurface environments, such as sediments and soils [158]. Recent studies have shown that the oxidation of Fe(II)-containing clay minerals, such as smectites [72] (particularly reduced nontronite [159,160]) and illite [161], is one of the important sources of environmental radicals, which deeply affects the attenuation behavior of pollutants, including 1,4-dioxane, TCE, phenol, and PAHs (Table 6). The iron contents in these clay minerals, which range from about 2 wt.% in montmorillonite to about 30 wt.% in nontronite [162], is a crucial factor influencing the ROS yield [72]. In addition to total Fe content, the different forms of Fe species in Fe-containing clay minerals, including structural Fe(II), surface-bound Fe(II), and exchangeable Fe(II), also have a significant impact on the generation of ROS. Structural Fe(II) is generally the dominant species for O_2 activation by Fe-containing clay minerals [163,164]. The reactivity of structural Fe(II) is highly affected by its coordination environment. Specifically, structural Fe(II) at the edge ($Fe(II)_{edge}$) is coordinated by electron-rich ligands (e.g., ≡O–, ≡HO–, and ≡Fe(II)–O–), which exhibit high activity for O_2 activation and preferentially lead to the generation of Fe(IV), along with a low •OH yield (Figure 3a). In contrast, interior Fe(II) ($Fe(II)_{int}$) tends to be coordinated by electron-poor ligands (e.g., ≡Al(III)–O– and ≡Fe(III)–O–). Although $Fe(II)_{int}$ is much less active than $Fe(II)_{edge}$, it can selectively activate O_2 to •OH [165]. Additionally, the $Fe(III)_{edge}$ can be regenerated through various pathways, such as the continuous supply of electrons from interior adjacent Fe(II) via single-electron transfer until the electrons in the interior Fe(II) are eventually depleted [72,166].

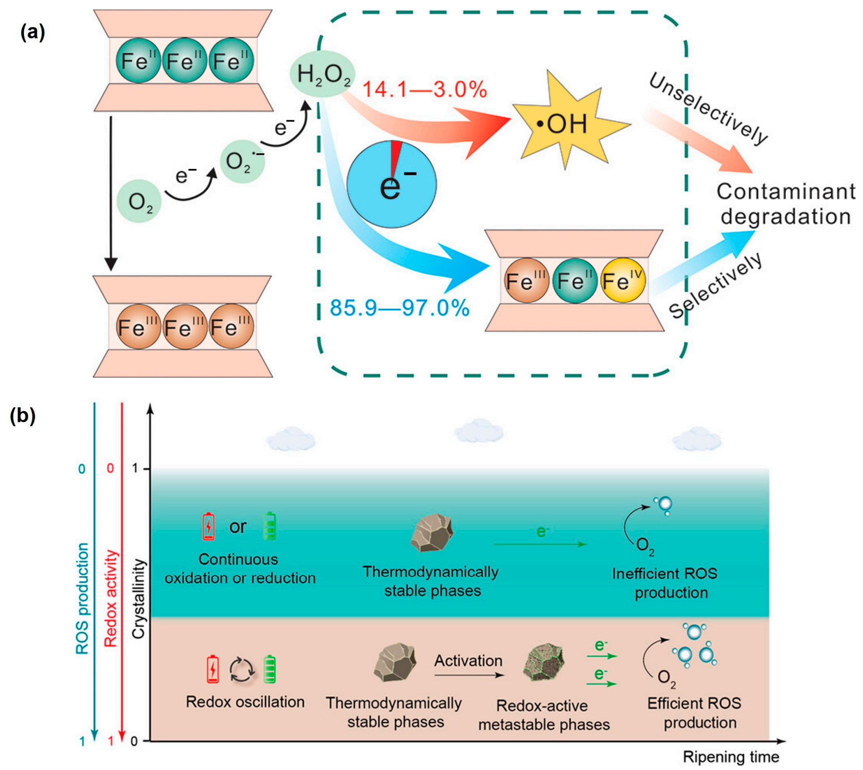

Figure 3. (**a**) Illustration of edge surface Fe(II) in clay mineral favoring the Fe(IV) generation over •OH generation [165]. (**b**) Illustration of redox oscillations activating thermodynamically stable iron minerals for enhanced ROS production [167].

Table 6. Degradation of organic pollutants via O_2 activation by Fe(II)-containing clay minerals and soils/sediments.

Material	Pollutant	Removal Ratio (%)	Reaction Time (h)	pH	Rate Constant	Reference
Nontronite	1,4-Dioxane	78.8 *	120	7.0	N/A	[161]
Illite	1,4-Dioxane	34.3 *	120	7.0	N/A	[161]
Montmorillonite	1,4-Dioxane	27.4 *	120	7.0	N/A	[161]
Reduced nontronite	Trichloroethylene	50.0	0.5	7.5	N/A	[160]
Riparian sediment	Trichloroethylene	27.6	6	7.0	N/A	[164]
Lakeshore sediment	Trichloroethylene	19.1	6	7.0	N/A	[164]
Pond sediment	Trichloroethylene	15.4	6	7.0	N/A	[164]
Nontronite	Phenol	43.1	6	7.0	N/A	[165]
Montmorillonite	Phenol	59.8	6	7.3	N/A	[165]
Sandbeach sediment	Phenol	9.95 *	10	6.96	N/A	[168]
Lakeshore sediment	Phenol	39.3 *	10	7.15	N/A	[168]
Farmland sediment	Phenol	48.5 *	10	Unadjusted	N/A	[168]
Paddy soils	Naphthalene	76.0 *	252	Unadjusted	N/A	[169]
Paddy soils	Phenanthrene	49.6 *	252	Unadjusted	N/A	[169]
Paddy soils	Pyrene	28.6 *	252	Unadjusted	N/A	[169]

Note: N/A, data not available. *, data obtained from the literature using the Getdata 2.26 software.

In addition to structural Fe(II), surface-bound Fe(II) also plays an important role in ROS generation and pollutant degradation by Fe(II)-containing clay minerals [168]. Similar to structural Fe(II), the reactivity of surface-bound Fe(II) is also highly dependent on its coordination environment. Specifically, the sequence of surface-bound Fe(II) reactivity probably follows the order of ≡Si(IV)–O–Fe(II) < ≡Al(III)–O–Fe(II) < ≡Fe(III)–O–Fe(II) < ≡Fe(II)–O–Fe(II) < ≡HO–Fe(II) [169]. Additionally, the coordination environment of surface-bound Fe(II) also affects the O_2-activation mechanism. When surface-bound Fe(II) is coordinated with electron-rich ligands, it can efficiently activate O_2. Nonetheless, due to the inner-sphere complexation with O_2, more non-•OH species (e.g., Fe(IV)) are generated. Conversely, when coordinated with electron-poor ligands, surface-bound Fe(II) exhibits a low reactivity toward O_2, but more •OH is generated, via an outer-sphere interaction mechanism with O_2 [168,169]. Compared to structural Fe(II) and surface-bound Fe(II), exchangeable Fe(II) contributes minimally to •OH formation and can even exhibit a scavenging effect against •OH [169].

In addition to engineered Fe-based materials and isolated Fe-bearing minerals, recent studies have increasingly focused on the generation of ROS in actual soils and sediments under the redox-fluctuation condition, and Fe(II)-bearing compounds play key roles in this process [164,170–175]. The soil–water interface was generally considered as the active zone for intense H_2O_2 and •OH production due to the limited oxygen penetration and the rapid turnover of the reducing and oxidizing substances at the redox interfaces [170,171]. Although the yield of ROS varies across different sediments due to their unique physicochemical properties, for specific sediment, surface-bound Fe(II) and structural Fe(II) in poorly crystalline iron minerals are the primary contributors to ROS production [168,176]. Model studies indicate that the relative contributions of surface-adsorbed Fe(II) and structural Fe(II) in •OH production are 16.4–33.9% and 66.1–83.6% in sediment, respectively [164]. It has recently been proposed that tidal hydrology-triggered redox fluctuation could promote ROS generation by accelerating the production of reactive ferrous ions and amorphous ferric oxyhydroxides, thereby promoting surface electrochemical activities and O_2-activation capability (Figure 3b) [167]. These results further confirm the vital role of natural iron minerals in ROS generation under dark conditions.

3. Influencing Factors

The efficiency of O_2 activation by iron-based materials is influenced by several key environmental or operational factors, including O_2 concentration, organic ligands, inorganic anions, and microbial activity. Moreover, some factors can change the O_2-activation mechanism and pathways. This section summarizes the effects of these factors on the efficiency and mechanisms of O_2 activation by iron-based materials.

3.1. O_2 Concentration

With O_2 being the precursor to the generated ROS, increasing the O_2 concentration commonly results in a higher ROS concentration during O_2 activation by Fe-based materials [69,70,72]. However, it has been reported that, for Fe-containing clay minerals, excessively high levels of O_2 would lead to adverse effects on the generation of ROS due to the ineffective oxidation of structural Fe(II) [177]. Additionally, in systems where oxidation and reduction transformation processes of pollutants occur simultaneously, the concentration of O_2 also influences the reaction pathway and products of organic pollutants. For example, in the aerobic degradation of TCE by ferrous minerals in natural sediments, more low-molecular-weight acids were generated when O_2 concentration exceeded 120 μM, while only acetylene and/or ethene were observed when O_2 concentration was lower than 26 μM [178]. Furthermore, O_2 concentration also affects the transformation behaviors of the iron-bearing minerals. For example, high O_2 concentration promotes the dissolution of FeS and facilitates the formation of reactive iron hydroxides/oxides, such as lepidocrocite, while Fe_3S_4 is generated in the absence of O_2 [144]. These O_2-concentration-dependent transformation products exhibit different capabilities in generating ROS such as •OH [144].

3.2. Organic Ligands

Both natural and synthetic organic ligands exist in the subsurface environment and significantly affect the efficiency of Fe-based materials in mediating O_2 activation. In general, synthetic organic ligands have greater influences on O_2 activation than natural ligands. Synthetic organic ligands, such as ethylenediaminetetraacetic acid (EDTA) and N,N′-1,2-ethanediylbis-1-aspartic acid (NTA), are well known for their outstanding ability to form stable complexes with iron ions across a wide pH range (Figure 4a) [179], thereby influencing Fe(II) oxidation kinetics and the iron cycle via modifying the redox potential [180,181]. Furthermore, these ligands have been found to promote the release of active iron species from the bulk materials through surface-polarization reactions [182] or the proton-coupled electron-transfer process (Figure 4b) [183–185]. The release of Fe into the aqueous solution depends on the concentration and complexing ability of ligands (Table 7) [83,186,187]. Specifically, EDTA, which has a particularly strong complexation ability, can form monodentate inner-sphere Fe(II)-EDTA complexes on the surface ZVI. When the concentration of EDTA is significantly lower than that of ZVI, only low levels of dissolved Fe(II) are detected in the solution. In this case, a heterogeneous reaction dominated by $Fe(II)_{ad}$–EDTA complexes is responsible for O_2 activation and ROS generation [188]. However, when the dosages of EDTA and ZVI are on the same order of magnitude, the $Fe(II)_{aq}$–EDTA complex in the solution predominantly drives the reactions, and free •OH in the solution is primarily responsible for removing organic pollutants [184]. Additionally, the configurations of the Fe–ligand complexes also significantly affect the efficiency of O_2 activation. For example, the Fe(II)–NTA complex is more efficient in activating O_2 than the Fe(II)–EDTA complex due to the relatively open structure, leading to more ROS generation under the same condition [188]. Moreover, some organic ligands with reducing capabilities, such as hydroxylamine [189], can even directly reduce Fe(III) to Fe(II), resulting in a more efficient Fe cycle and higher ROS yield. Notably, the quenching effect of the ligands on •OH (Table 7) should be also considered for a more accurate analysis of the contributions of ROS to pollutant degradation kinetics.

Table 7. Stability constants of Fe(II)/Fe(III)-complexes with common organic ligands and rate constants for reaction of these ligands with •OH.

Species	Log β of Fe(II)-Complex	Log β of Fe(III)-Complex	Reaction Rate Constants with •OH (M^{-1} s^{-1})	Reference
EDTA	14.3	25.1	2.0×10^9	[83]
EDDS	N/A	20.6	2.5×10^9	[83,187]
NTA	8.05	15.90	5.5×10^8	[83,186]
CA	3.2	8.36–12.38 and 11.5	3.2×10^8	[83]
OA	> 4.70	9.4	1.0×10^7	[83]
HA	N/A	6.65–7.59	N/A	[83]

Note: N/A, data not available.

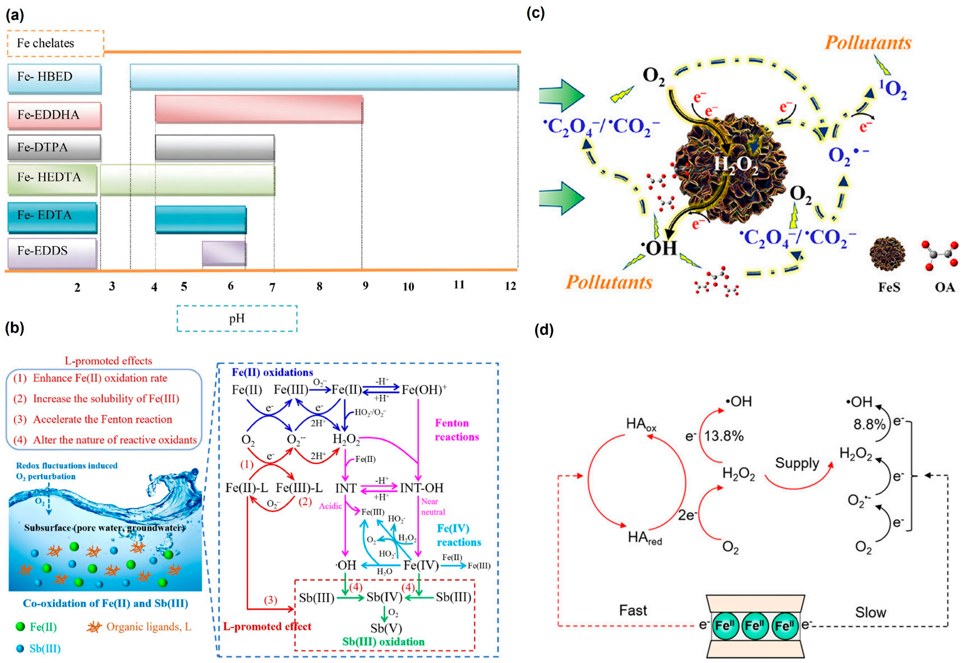

Figure 4. (**a**) Summary of pH ranges over which Fe chelates are stable [179]. (**b**) Reaction mechanisms of ligand-enhanced Fe(II) oxidation [183]. (**c**) Illustration of OA-enhanced FeS oxygenation mechanism [190]. (**d**) Illustration of the mechanisms for HA-enhanced oxygenation of Fe-containing clay mineral [191].

Compared to synthetic ligands, natural organic acids, including citric acid (CA), oxalate (OA), and humic acid (HA), generally exhibit a relatively weak ability to form complexes with iron. However, they can still modify the redox potential of iron ions and accelerate the iron cycle and O_2 activation effectively [192]. Moreover, reductive natural organic acids, such as glutathione [193], ascorbic acid [194], and protocatechuic acid [195], have the potential to reduce Fe(III) to Fe(II) directly. Studies have indicated that the dissolved Fe(II)–ligand complexes can mediate one electron-transfer process and play a dominant role in O_2 activation by FeS in the presence of CA and OA [192]. However, the capability of these organic acids to promote the dissolution of FeS_2 is lower than for FeS due to the more stable structure of FeS_2. Correspondingly, dissolved Fe(II)-mediated O_2 activation is less important in FeS_2 suspension [182,192]. These results indicated that the effect of organic acids on the contribution of homogeneous reactions to overall O_2 activation efficiency is closely related to the properties of the materials. Notably, it was recently revealed that organic ligands can promote ROS generation during the oxygenation of FeS minerals by producing abundant carbon-centered radicals. For example, OA could be preferentially oxidized by •OH, leading to the generation of carbon-centered radicals (e.g., $\bullet C_2O_4^-$ and $\bullet CO_2^-$), which further supply electrons to O_2 and contribute to at least 93.6% of the total •OH production in the FeS/OA/O_2 system (Figure 4c) [190].

As an important constituent of natural organic matter, HA has been confirmed to promote the generation of •OH by forming an aqueous Fe–HA complex and promoting the regeneration of Fe(II) via its reduced functional groups [196–199]. Meanwhile, microbially or chemically reduced HA has the potential to directly activate O_2 via the active quinone groups (−137 to −225 mV vs. NHE) to generate ROS [200]. Moreover, HA can mediate heterogeneous O_2 activation by Fe-containing minerals. It has been recently proposed that the presence of HA could change the reaction mechanism of nontronite oxygenation, where HA accepts electrons from the structural Fe and then delivers the elections to O_2 through two-electron-transfer pathways (Figure 4d) [191]. Compared to the direct electron transfer from structural Fe to O_2, reduced HA exhibits a faster O_2-reduction rate and higher selectivity for •OH. The HA-mediated pathways contributed to 70% of H_2O_2 and 62.1% of •OH generation in the HA/nontronite system. However, other studies have shown that the presence of HA could slow down the oxidation of reduced Fe-bearing clay minerals due to the competitive adsorption with O_2 [201].

Organic ligands can also affect the generation of non-hydroxyl radical species during the Fe-based material-mediated O_2-activation process. For example, the presence of CA could promote the generation of $^1O_2$ in the S–nZVI/O_2 systems because the Fe(II)–CA complex promotes the generation of more $O_2^{\bullet-}$, which could further react with H_2O/H^+ to generate $^1O_2$ and H_2O_2 [202].

3.3. Inorganic Anions

Inorganic anions are prevalent in the subsurface environment and play a significant role in influencing the oxidation behavior of Fe-based materials, mainly by inducing aggregation, increasing the hydrodynamic diameter, and competing with ROS [110]. Studies have shown that the inhibitory effects of common inorganic anions on O_2 activation by Fe-based materials, such as S–nZVI and nZVI, can be ranked in the order of $Cl^- < NO_3^- < SO_4^{2-} < HCO_3^- < HPO_4^{2-}$. This discrepancy could be primarily attributed to the varying degrees of competition that these anions exhibit with ROS [203]. Moreover, for Cl^-, its reaction with •OH to generate secondary chlorine radicals, such as $Cl^\bullet$, $Cl_2^{\bullet-}$, and $ClOH^{\bullet-}$ (Table 8), can partially mitigate the negative effects caused by •OH consumption. The impact of these inorganic anions on the degradation of organic pollutants also depends on the concentrations of the anions and ROS. For a FeS suspension exposed to air, 5 mg/L of Cl^- significantly hinders •OH generation. However, with sufficient O_2 (e.g., through O_2 purging of the suspension), even 500 mg/L of Cl^- has a limited effect on •OH concentration in the suspension due to the abundance of ROS involved in the •OH generation process. Interestingly, the addition of 50,000 mg/L Cl^- has been reported to enhance •OH generation, likely due to the production of secondary chlorine radicals [144]. Particularly noteworthy is the effect of the orthophosphate ion (PO_4^{3-}), which could adsorb on the surface of Fe minerals (e.g., green rust) and form the $[FeII(OH)_2\text{-}PO_4]^{3-}$ complex (Figure 5a), facilitating O_2 activation and the generation of $O_2^{\bullet-}$ [204]. When PO_4^{3-} is introduced to an aerated suspension of surface-oxidized ZVI ($Fe@Fe_2O_3$), the PO_4^{3-} ions can change the O_2-reduction pathway from a four-electron to a one-electron process (Figure 5b) [205]. Moreover, the surface phosphate layer induces the in situ generation of atomic hydrogen (•H) on the $Fe@Fe_2O_3$ surface, which can further promote the sequential one-electron O_2-reduction pathway (Figure 5b) [205].

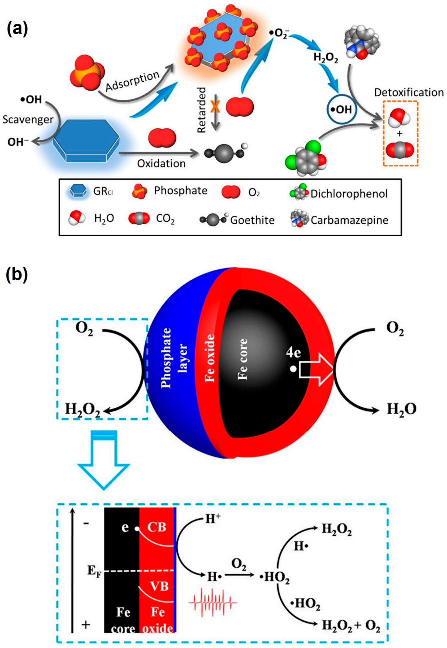

Figure 5. (**a**) Illustration of phosphate-enhanced O_2 activation by green rust [204]. (**b**) Illustration of phosphate-enhanced O_2 activation in $Fe@Fe_2O_3$ system [205].

Table 8. Reaction rate constants between •OH and inorganic anions.

Reaction	Rate Constant ($M^{-1}\ s^{-1}$)	Reference
$Cl^- + \bullet OH \rightarrow ClOH^{\bullet -}$	4.3×10^9	[206]
$ClOH^{\bullet -} \rightarrow Cl^- + \bullet OH$	6.1×10^9	[206]
$ClOH^{\bullet -} + H^+ \rightarrow Cl^\bullet + H_2O$	4.3×10^{10}	[206]
$Cl^\bullet + Cl^- \rightarrow Cl_2^{\bullet -}$	1.0×10^5	[206]
$\bullet OH + HCO_3^- \rightarrow CO_3^{\bullet -} + H_2O$	8.5×10^6	[207]
$\bullet OH + CO_3^{2-} \rightarrow CO_3^{\bullet -} + OH^-$	3.9×10^8	[206]
$HPO_4^{2-} + \bullet OH \rightarrow HPO_4^{\bullet -} + OH^-$	8.0×10^5	[206]

3.4. Microbial Activity

Microbially mediated iron redox reactions are crucial geochemical processes in the environment [208]. Although the presence of O_2 can lead to a 38–64% decrease in the abundance of iron-reducing bacteria, these microorganisms can recover to 121–793% of their original levels after the restoration of anoxic conditions [209]. Therefore, the role of microorganisms in redox dynamics should garner more attention. Iron-reducing microorganisms could enhance the cycle of Fe(II)/Fe(III) via direct electron transfer [210], serving as extracellular electron shuttles [211] and releasing reduced species (e.g., flavins) [212,213], thus leading to a continuous supply of Fe(II) and a higher ROS yield. Notably, the extent of Fe(III) reduction is related to the mineral composition. For example, goethite with lower crystallinity is preferentially reduced compared to illite by *Shewanella putrefaciens* CN32, a metal-reducing bacterium [213]. Sulfate-reducing microorganisms also have important effects on the iron cycle [214]. Additionally, the presence of certain bacteria, such as neutrophilic iron-oxidizing bacteria [215], can alter the surface properties of Fe minerals and result in the renewal of mineral surfaces through continuous oxidative dissolution [216]. This microbially mediated transformation of iron minerals has significant impacts on O_2 activation by these minerals.

4. Conclusions and Perspectives

Iron-based materials have demonstrated significant potential in activating O_2 for in situ remediation of sites with organic contaminants. This review systematically examines the current research on O_2 activation by ZVI, iron sulfide, iron oxide, and Fe-bearing clay minerals. Notably, we have summarized recent findings about the roles of Fe-bearing components in natural soils and sediments for O_2 activation and ROS generation. The mechanisms for O_2 activation by these Fe-based materials are thoroughly discussed, including the active sites/species, electron-transfer pathways, and transformation of the materials, and the environmental and operational factors influencing O_2 activation and ROS generation are analyzed. Despite these significant advances, O_2 activation by Fe-based materials has not yet been applied for in situ remediation of organic-contaminated sites. Further investigations are needed to address the potential limitations of this promising remediation technology and overcome the barriers to its real-world application:

1. The ROS-generation dynamics under environmental conditions need thorough elucidation and characterization to achieve more accurate prediction and precise control of pollutant removal performance in practical applications. Current studies have demonstrated that the major reactive species generated in O_2 activation by Fe-based materials are H_2O_2, •OH, and $O_2^{\bullet -}$. However, the potential contribution of other reactive species, especially $^1O_2$, should be further explored, which has shown tremendous potential in selective oxidation of various contaminants [217,218]. Meanwhile, high-resolution monitoring of ROS-generation dynamics in actual subsurface environments is indispensable, which requires further exploration of novel tools suitable for in situ analysis of trace-level ROS. A notable example of such analytical tools is flow-injection chemiluminescence analysis, which can be performed with a portable device, achieving on-site quantification of •OH in environmental matrices [219].

2. While O_2 activation by Fe-based materials can degrade a variety of organic pollutants (e.g., TCE, PAHs, phenols, organic dyes, and antibiotics), future efforts are needed to explore its potential for degrading recalcitrant emerging pollutants (e.g., PFASs). The configuration of surface iron sites and interfacial microenvironment significantly affect the efficiency of O_2 activation. Further research is needed to elucidate the relationship between the functional groups of pollutants and the electron-shuttle mechanism for the tailored development of efficient Fe-based materials for the removal of emerging pollutants. For example, •OH is ineffective in degrading PFASs, whereas $O_2^{\bullet-}$ has demonstrated the capability to degrade perfluorocarboxylic acids with varying chain lengths [220]. Although $O_2^{\bullet-}$ is an easily formed intermediate during O_2 activation by Fe-based materials, it is quickly converted to other ROS. Therefore, nanotechnology-enabled rational material design is needed to manipulate the generation and consumption pathways of $O_2^{\bullet-}$ during O_2 activation and improve its selectivity toward reaction with PFASs. This can benefit from theoretical simulations of the interaction between the material surface and O_2/pollutant molecules under environmentally realistic conditions. Furthermore, the rational design of Fe-based materials for controllable O_2 activation and ROS generation can be substantially expedited by incorporating machine-learning analysis of large datasets on the structure–reactivity relationships [221,222].
3. Attention should be directed toward conducting pilot-scale applications of this technology to validate its effectiveness in real-world scenarios. In particular, for remediating contaminated sites lacking reactive Fe minerals, it is necessary to introduce Fe-based materials capable of efficient O_2 activation. Iron-based materials that show excellent performance in laboratory studies may not work when applied in real aquifers, and it is vital to ensure that mass-produced remediation agents exhibit activity comparable to those tested in the initial research and development (R&D) stage. Moreover, the effective delivery of these Fe-based remediation agents can be a bottleneck for ISCO remediation via Fe-mediated O_2 activation. This calls for a simultaneous evaluation of the transport properties of the Fe-based materials while optimizing their O_2 activation efficiency.
4. In addition to the above technical challenges, other barriers to the real-world applications of O_2 activation for site remediation need to be overcome. To be economically viable and competitive, costs associated with the materials, equipment, and power need to be lowered. While Fe is an earth-abundant element, the R&D and scale-up production of sophisticated Fe-based materials still may be costly. Moreover, despite the abundance and availability of O_2 in the air, the energy required to deliver it into deep aquifers adds to the total cost of this technology. Finally, since Fe-based materials (e.g., nZVI) have shown toxicity to a variety of soil organisms [223–225], it is critical to evaluate the potential environmental impact of these materials before they can be safely applied in the subsurface environment. A comprehensive consideration of these factors is warranted to ensure the successful utilization of O_2, a green and inexhaustible oxidant, for sustainable in situ remediation of organic-contaminated sites.

Author Contributions: F.H.: Investigation, Writing—original draft, Writing—review and editing. L.X.: Investigation, Validation. H.W.: Writing—review and editing, Funding acquisition, Project administration. C.J.: Writing—review and editing, Funding acquisition, Supervision, Conceptualization. All authors have read and agreed to the published version of the manuscript.

Funding: This research was funded by the National Natural Science Foundation of China (22276101, 52370053), Tianjin Municipal Science and Technology Bureau (23JCZDJC00740), and the Fundamental Research Funds for the Central Universities (63241632).

Institutional Review Board Statement: Not applicable.

Informed Consent Statement: Not applicable.

Data Availability Statement: No new data were created or analyzed in this study. Data sharing is not applicable to this article.

Conflicts of Interest: The authors declare no conflicts of interest.

References

1. Bunting, S.Y.; Lapworth, D.J.; Crane, E.J.; Grima-Olmedo, J.; Koroša, A.; Kuczyńska, A.; Mali, N.; Rosenqvist, L.; Van Vliet, M.E.; Togola, A.; et al. Emerging Organic Compounds in European Groundwater. *Environ. Pollut.* **2021**, *269*, 115945. [CrossRef] [PubMed]
2. Hua, T.; Propp, V.R.; Power, C.; Brown, S.J.; Collins, P.; Smith, J.E.; Roy, J.W. Multizone Aquatic Ecological Exposures to Landfill Contaminants from a Groundwater Plume Discharging to a Pond. *Environ. Toxicol. Chem.* **2023**, *42*, 1667–1684. [CrossRef] [PubMed]
3. Jia, X.; O'Connor, D.; Hou, D.; Jin, Y.; Li, G.; Zheng, C.; Ok, Y.S.; Tsang, D.C.W.; Luo, J. Groundwater Depletion and Contamination: Spatial Distribution of Groundwater Resources Sustainability in China. *Sci. Total Environ.* **2019**, *672*, 551–562. [CrossRef] [PubMed]
4. Kumar, M.; Goswami, R.; Patel, A.K.; Srivastava, M.; Das, N. Scenario, Perspectives and Mechanism of Arsenic and Fluoride Co-Occurrence in the Groundwater: A Review. *Chemosphere* **2020**, *249*, 126126. [CrossRef] [PubMed]
5. Abiriga, D.; Vestgarden, L.S.; Klempe, H. Groundwater Contamination from a Municipal Landfill: Effect of Age, Landfill Closure, and Season on Groundwater Chemistry. *Sci. Total Environ.* **2020**, *737*, 140307. [CrossRef] [PubMed]
6. Propp, V.R.; De Silva, A.O.; Spencer, C.; Brown, S.J.; Catingan, S.D.; Smith, J.E.; Roy, J.W. Organic Contaminants of Emerging Concern in Leachate of Historic Municipal Landfills. *Environ. Pollut.* **2021**, *276*, 116474. [CrossRef] [PubMed]
7. Sun, Y.; Li, H.; Lei, S.; Semple, K.T.; Coulon, F.; Hu, Q.; Gao, J.; Guo, G.; Gu, Q.; Jones, K.C. Redevelopment of Urban Brownfield Sites in China: Motivation, History, Policies and Improved Management. *Eco-Environ. Health* **2022**, *1*, 63–72. [CrossRef] [PubMed]
8. Wu, S.; Xiang, Z.; Lin, D.; Zhu, L. Multimedia Distribution and Health Risk Assessment of Typical Organic Pollutants in a Retired Industrial Park. *Front. Environ. Sci. Eng.* **2023**, *17*, 142. [CrossRef]
9. Moran, M.J.; Zogorski, J.S.; Squillace, P.J. Chlorinated Solvents in Groundwater of the United States. *Environ. Sci. Technol.* **2007**, *41*, 74–81. [CrossRef]
10. Bulatović, S.; Ilić, M.; Šolević Knudsen, T.; Milić, J.; Pucarević, M.; Jovančićević, B.; Vrvić, M.M. Evaluation of Potential Human Health Risks from Exposure to Volatile Organic Compounds in Contaminated Urban Groundwater in the Sava River Aquifer, Belgrade, Serbia. *Environ. Geochem. Health* **2022**, *44*, 3451–3472. [CrossRef]
11. Montuori, P.; De Rosa, E.; Cerino, P.; Pizzolante, A.; Nicodemo, F.; Gallo, A.; Rofrano, G.; De Vita, S.; Limone, A.; Triassi, M. Estimation of Polycyclic Aromatic Hydrocarbons in Groundwater from Campania Plain: Spatial Distribution, Source Attribution and Health Cancer Risk Evaluation. *Toxics* **2023**, *11*, 435. [CrossRef] [PubMed]
12. Peng, B.; Dong, Q.; Li, F.; Wang, T.; Qiu, X.; Zhu, T. A Systematic Review of Polycyclic Aromatic Hydrocarbon Derivatives: Occurrences, Levels, Biotransformation, Exposure Biomarkers, and Toxicity. *Environ. Sci. Technol.* **2023**, *57*, 15314–15335. [CrossRef] [PubMed]
13. Li, M.; Chen, Q.; Yang, L.; Zhang, Y.; Jiang, J.; Deng, S.; Wan, J.; Fan, T.; Long, T.; Zhang, S.; et al. Contaminant Characterization at Pesticide Production Sites in the Yangtze River Delta: Residue, Distribution, and Environmental Risk. *Sci. Total Environ.* **2023**, *860*, 160156. [CrossRef] [PubMed]
14. Huo, Z.; Xi, M.; Xu, L.; Jiang, C.; Chen, W. Colloid-Facilitated Release of Polybrominated Diphenyl Ethers at an e-Waste Recycling Site: Evidence from Undisturbed Soil Core Leaching Experiments. *Front. Environ. Sci. Eng.* **2024**, *18*, 21. [CrossRef]
15. Schaefer, C.E.; Lavorgna, G.M.; Lippincott, D.R.; Nguyen, D.; Schaum, A.; Higgins, C.P.; Field, J. Leaching of Perfluoroalkyl Acids during Unsaturated Zone Flushing at a Field Site Impacted with Aqueous Film Forming Foam. *Environ. Sci. Technol.* **2023**, *57*, 1940–1948. [CrossRef] [PubMed]
16. Stroo, H.F.; Unger, M.; Ward, C.H.; Kavanaugh, M.C.; Vogel, C.; Leeson, A.; Marqusee, J.A.; Smith, B.P. Remediating Chlorinated Solvent Source Zones. *Environ. Sci. Technol.* **2003**, *37*, 224A–230A. [CrossRef]
17. Cheng, Y.; Zhu, J. Significance of Mass–Concentration Relation on the Contaminant Source Depletion in the Nonaqueous Phase Liquid (NAPL) Contaminated Zone. *Transp. Porous Med.* **2021**, *137*, 399–416. [CrossRef]
18. Tatti, F.; Papini, M.P.; Sappa, G.; Raboni, M.; Arjmand, F.; Viotti, P. Contaminant Back-Diffusion from Low-Permeability Layers as Affected by Groundwater Velocity: A Laboratory Investigation by Box Model and Image Analysis. *Sci. Total Environ.* **2018**, *622–623*, 164–171. [CrossRef]
19. Ma, T.; Pan, X.; Wang, T.; Li, X.; Luo, Y. Toxicity of Per- and Polyfluoroalkyl Substances to Nematodes. *Toxics* **2023**, *11*, 593. [CrossRef]
20. Ge, Y.; Wang, Z.; Chen, X.; Wang, W.; Liu, Z.; Sun, H.; Zhang, L. Comparative Toxicological Effects of Perfluorooctane Sulfonate and Its Alternative 6:2 Chlorinated Polyfluorinated Ether Sulfonate on Earthworms. *Environ. Toxicol. Chem.* **2023**, *43*, 170–181. [CrossRef]
21. Ordaz, J.D.; Damayanti, N.P.; Irudayaraj, J.M.K. Toxicological Effects of Trichloroethylene Exposure on Immune Disorders. *Immunopharmacol. Immunotoxicol.* **2017**, *39*, 305–317. [CrossRef] [PubMed]

22. Grazuleviciene, R.; Nieuwenhuijsen, M.J.; Vencloviene, J.; Kostopoulou-Karadanelli, M.; Krasner, S.W.; Danileviciute, A.; Balcius, G.; Kapustinskiene, V. Individual Exposures to Drinking Water Trihalomethanes, Low Birth Weight and Small for Gestational Age Risk: A Prospective Kaunas Cohort Study. *Environ. Health* **2011**, *10*, 32. [CrossRef] [PubMed]
23. Han, Y.; Cheng, J.; He, L.; Zhang, M.; Ren, S.; Sun, J.; Xing, X.; Tang, Z. Polybrominated Diphenyl Ethers in Soils from Tianjin, North China: Distribution, Health Risk, and Temporal Trends. *Environ. Geochem. Health* **2021**, *43*, 1177–1191. [CrossRef] [PubMed]
24. Sankar, T.K.; Kumar, A.; Mahto, D.K.; Das, K.C.; Narayan, P.; Fukate, M.; Awachat, P.; Padghan, D.; Mohammad, F.; Al-Lohedan, H.A.; et al. The Health Risk and Source Assessment of Polycyclic Aromatic Hydrocarbons (PAHs) in the Soil of Industrial Cities in India. *Toxics* **2023**, *11*, 515. [CrossRef] [PubMed]
25. Daraban, G.M.; Hlihor, R.-M.; Suteu, D. Pesticides vs. Biopesticides: From Pest Management to Toxicity and Impacts on the Environment and Human Health. *Toxics* **2023**, *11*, 983. [CrossRef]
26. Horzmann, K.A.; Portales, A.M.; Batcho, K.G.; Freeman, J.L. Developmental Toxicity of Trichloroethylene in Zebrafish (*Danio Rerio*). *Environ. Sci. Processes Impacts* **2020**, *22*, 728–739. [CrossRef]
27. Yan, Z.G.; Li, Z.G.; Du, J.Z. Effects of Environmental Organic Pollutants on Environment and Human Health: The Latest Updates. *Toxics* **2024**, *12*, 231. [CrossRef]
28. Wang, J.; Chen, S.; Tian, M.; Zheng, X.; Gonzales, L.; Ohura, T.; Mai, B.; Simonich, S.L.M. Inhalation Cancer Risk Associated with Exposure to Complex Polycyclic Aromatic Hydrocarbon Mixtures in an Electronic Waste and Urban Area in South China. *Environ. Sci. Technol.* **2012**, *46*, 9745–9752. [CrossRef]
29. Mahoney, H.; Xie, Y.; Brinkmann, M.; Giesy, J.P. Next Generation Per- and Poly-Fluoroalkyl Substances: Status and Trends, Aquatic Toxicity, and Risk Assessment. *Eco-Environ. Health* **2022**, *1*, 117–131. [CrossRef]
30. Palazzolo, S.; Caligiuri, I.; Sfriso, A.A.; Mauceri, M.; Rotondo, R.; Campagnol, D.; Canzonieri, V.; Rizzolio, F. Early Warnings by Liver Organoids on Short- and Long-Chain PFAS Toxicity. *Toxics* **2022**, *10*, 91. [CrossRef]
31. Stroo, H.F.; Leeson, A.; Marqusee, J.A.; Johnson, P.C.; Ward, C.H.; Kavanaugh, M.C.; Sale, T.C.; Newell, C.J.; Pennell, K.D.; Lebrón, C.A.; et al. Chlorinated Ethene Source Remediation: Lessons Learned. *Environ. Sci. Technol.* **2012**, *46*, 6438–6447. [CrossRef] [PubMed]
32. Cheng, M.; Zeng, G.; Huang, D.; Lai, C.; Xu, P.; Zhang, C.; Liu, Y. Hydroxyl Radicals Based Advanced Oxidation Processes (AOPs) for Remediation of Soils Contaminated with Organic Compounds: A Review. *Chem. Eng. J.* **2016**, *284*, 582–598. [CrossRef]
33. Liu, J.W.; Wei, K.H.; Xu, S.W.; Cui, J.; Ma, J.; Xiao, X.L.; Xi, B.D.; He, X.S. Surfactant-Enhanced Remediation of Oil-Contaminated Soil and Groundwater: A Review. *Sci. Total Environ.* **2021**, *756*, 144142. [CrossRef] [PubMed]
34. Tsitonaki, A.; Petri, B.; Crimi, M.; Mosbæk, H.; Siegrist, R.L.; Bjerg, P.L. In Situ Chemical Oxidation of Contaminated Soil and Groundwater Using Persulfate: A Review. *Crit. Rev. Environ. Sci. Technol.* **2010**, *40*, 55–91. [CrossRef]
35. Ranc, B.; Faure, P.; Croze, V.; Simonnot, M.O. Selection of Oxidant Doses for in Situ Chemical Oxidation of Soils Contaminated by Polycyclic Aromatic Hydrocarbons (PAHs): A Review. *J. Hazard. Mater.* **2016**, *312*, 280–297. [CrossRef]
36. Wei, K.H.; Ma, J.; Xi, B.-D.; Yu, M.D.; Cui, J.; Chen, B.L.; Li, Y.; Gu, Q.B.; He, X.S. Recent Progress on In-Situ Chemical Oxidation for the Remediation of Petroleum Contaminated Soil and Groundwater. *J. Hazard. Mater.* **2022**, *432*, 128738. [CrossRef]
37. Liu, H.; Bruton, T.A.; Doyle, F.M.; Sedlak, D.L. In Situ Chemical Oxidation of Contaminated Groundwater by Persulfate: Decomposition by Fe(III)- and Mn(IV)-Containing Oxides and Aquifer Materials. *Environ. Sci. Technol.* **2014**, *48*, 10330–10336. [CrossRef]
38. Pan, C.; Wang, C.; Zhao, X.; Xu, P.; Mao, F.; Yang, J.; Zhu, Y.; Yu, R.; Xiao, S.; Fang, Y.; et al. Neighboring sp-Hybridized Carbon Participated Molecular Oxygen Activation on the Interface of Sub-Nanocluster CuO/Graphdiyne. *J. Am. Chem. Soc.* **2022**, *144*, 4942–4951. [CrossRef]
39. Wei, Y.; Chen, Y.; Cao, X.; Xiang, M.; Huang, Y.; Li, H. A Critical Review of Groundwater Table Fluctuation: Formation, Effects on Multifields, and Contaminant Behaviors in a Soil and Aquifer System. *Environ. Sci. Technol.* **2024**, *58*, 2185–2203. [CrossRef]
40. Ji, J.; Wang, Z.; Xu, Q.; Zhu, Q.; Xing, M. In Situ H_2O_2 Generation and Corresponding Pollutant Removal Applications: A Review. *Chem. Eur. J.* **2023**, *29*, e202203921. [CrossRef]
41. Guo, X.; Lin, S.; Gu, J.; Zhang, S.; Chen, Z.; Huang, S. Simultaneously Achieving High Activity and Selectivity toward Two-Electron O_2 Electroreduction: The Power of Single-Atom Catalysts. *ACS Catal.* **2019**, *9*, 11042–11054. [CrossRef]
42. Zheng, Y.; Yu, Z.; Ou, H.; Asiri, A.M.; Chen, Y.; Wang, X. Black Phosphorus and Polymeric Carbon Nitride Heterostructure for Photoinduced Molecular Oxygen Activation. *Adv. Funct. Mater.* **2018**, *28*, 1705407. [CrossRef]
43. Colombo, C.; Palumbo, G.; He, J.-Z.; Pinton, R.; Cesco, S. Review on Iron Availability in Soil: Interaction of Fe Minerals, Plants, and Microbes. *J. Soils Sediments* **2014**, *14*, 538–548. [CrossRef]
44. Guo, H.; Barnard, A.S. Naturally Occurring Iron Oxide Nanoparticles: Morphology, Surface Chemistry and Environmental Stability. *J. Mater. Chem. A* **2013**, *1*, 27–42. [CrossRef]
45. Wang, Y.; Jin, X.; Peng, A.; Gu, C. Transformation and Toxicity of Environmental Contaminants as Influenced by Fe Containing Clay Minerals: A Review. *Bull. Environ. Contam. Toxicol.* **2020**, *104*, 8–14. [CrossRef]
46. Gong, Y.; Tang, J.; Zhao, D. Application of Iron Sulfide Particles for Groundwater and Soil Remediation: A Review. *Water Res.* **2016**, *89*, 309–320. [CrossRef]
47. Zeng, G.; Wang, J.; Dai, M.; Meng, Y.; Luo, H.; Zhou, Q.; Lin, L.; Zang, K.; Meng, Z.; Pan, X. Natural Iron Minerals in an Electrocatalytic Oxidation System and in Situ Pollutant Removal in Groundwater: Applications, Mechanisms, and Challenges. *Sci. Total Environ.* **2023**, *871*, 161826. [CrossRef]

48. Quinn, J.; Geiger, C.; Clausen, C.; Brooks, K.; Coon, C.; O'Hara, S.; Krug, T.; Major, D.; Yoon, W.-S.; Gavaskar, A.; et al. Field Demonstration of DNAPL Dehalogenation Using Emulsified Zero-Valent Iron. *Environ. Sci. Technol.* **2005**, *39*, 1309–1318. [CrossRef]
49. Gu, Y.; Wang, B.; He, F.; Bradley, M.J.; Tratnyek, P.G. Mechanochemically Sulfidated Microscale Zero Valent Iron: Pathways, Kinetics, Mechanism, and Efficiency of Trichloroethylene Dechlorination. *Environ. Sci. Technol.* **2017**, *51*, 12653–12662. [CrossRef]
50. Xu, J.; Wang, Y.; Weng, C.; Bai, W.; Jiao, Y.; Kaegi, R.; Lowry, G.V. Reactivity, Selectivity, and Long-Term Performance of Sulfidized Nanoscale Zerovalent Iron with Different Properties. *Environ. Sci. Technol.* **2019**, *53*, 5936–5945. [CrossRef]
51. Brumovský, M.; Oborná, J.; Micić, V.; Malina, O.; Kašlík, J.; Tunega, D.; Kolos, M.; Hofmann, T.; Karlický, F.; Filip, J. Iron Nitride Nanoparticles for Enhanced Reductive Dechlorination of Trichloroethylene. *Environ. Sci. Technol.* **2022**, *56*, 4425–4436. [CrossRef] [PubMed]
52. Gong, L.; Chen, J.; Hu, Y.; He, K.; Bylaska, E.J.; Tratnyek, P.G.; He, F. Degradation of Chloroform by Zerovalent Iron: Effects of Mechanochemical Sulfidation and Nitridation on the Kinetics and Mechanism. *Environ. Sci. Technol.* **2023**, *57*, 9811–9821. [CrossRef]
53. Chen, Z.; Chen, J.; Tan, S.; Yang, Z.; Zhang, Y. Dechlorination Helps Defluorination: Insights into the Defluorination Mechanism of Florfenicol by S-nZVI and DFT Calculations on the Reaction Pathways. *Environ. Sci. Technol.* **2024**, *58*, 2542–2553. [CrossRef] [PubMed]
54. Usman, M.; Faure, P.; Ruby, C.; Hanna, K. Remediation of PAH-Contaminated Soils by Magnetite Catalyzed Fenton-like Oxidation. *Appl. Catal. B* **2012**, *117–118*, 10–17. [CrossRef]
55. Liu, X.; Yuan, S.; Zhang, P.; Zhu, J.; Tong, M. Reduced Nontronite-Activated H_2O_2 for Contaminants Degradation: The Beneficial Role of Clayed Fractions in ISCO Treatments. *J. Hazard. Mater.* **2020**, *386*, 121945. [CrossRef] [PubMed]
56. Chen, N.; Fang, G.; Liu, G.; Zhou, D.; Gao, J.; Gu, C. The Effects of Fe-Bearing Smectite Clays on •OH Formation and Diethyl Phthalate Degradation with Polyphenols and H_2O_2. *J. Hazard. Mater.* **2018**, *357*, 483–490. [CrossRef]
57. Sun, Y.; Danish, M.; Ali, M.; Shan, A.; Li, M.; Lyu, Y.; Qiu, Z.; Sui, Q.; Zang, X.; Lyu, S. Trichloroethene Degradation by Nanoscale CaO_2 Activated with Fe(II)/FeS: The Role of FeS and the Synergistic Activation Mechanism of Fe(II)/FeS. *Chem. Eng. J.* **2020**, *394*, 124830. [CrossRef]
58. Kim, J.-G.; Kim, H.-B.; Jeong, W.-G.; Baek, K. Enhanced-Oxidation of Sulfanilamide in Groundwater Using Combination of Calcium Peroxide and Pyrite. *J. Hazard. Mater.* **2021**, *419*, 126514. [CrossRef]
59. Li, H.; Yao, Y.; Zhang, J.; Du, J.; Xu, S.; Wang, C.; Zhang, D.; Tang, J.; Zhao, H.; Zhou, J. Degradation of Phenanthrene by Peroxymonosulfate Activated with Bimetallic Metal-Organic Frameworks: Kinetics, Mechanisms, and Degradation Products. *Chem. Eng. J.* **2020**, *397*, 125401. [CrossRef]
60. Lee, Y.C.; Li, Y.; Chen, M.J.; Chen, Y.-C.; Kuo, J.; Lo, S.L. Efficient Decomposition of Perfluorooctanic Acid by Persulfate with Iron-Modified Activated Carbon. *Water Res.* **2020**, *174*, 115618. [CrossRef]
61. Dong, H.; He, Q.; Zeng, G.; Tang, L.; Zhang, L.; Xie, Y.; Zeng, Y.; Zhao, F. Degradation of Trichloroethene by Nanoscale Zero-Valent Iron (nZVI) and nZVI Activated Persulfate in the Absence and Presence of EDTA. *Chem. Eng. J.* **2017**, *316*, 410–418. [CrossRef]
62. Liu, H.; Fu, P.; Liu, F.; Hou, Q.; Tong, Z.; Bi, W. Degradation of Ciprofloxacin by Persulfate Activated with Pyrite: Mechanism, Acidification and Tailwater Reuse. *RSC Adv.* **2022**, *12*, 29991–30000. [CrossRef] [PubMed]
63. Liu, X.; Shao, P.; Gao, S.; Bai, Z.; Tian, J. Benzoquinone-Assisted Heterogeneous Activation of PMS on Fe_3S_4 via Formation of Active Complexes to Mediate Electron Transfer towards Enhanced Bisphenol A Degradation. *Water Res.* **2022**, *226*, 119218. [CrossRef] [PubMed]
64. Wang, Q.; Zeng, H.; Liang, Y.; Cao, Y.; Xiao, Y.; Ma, J. Degradation of Bisphenol AF in Water by Periodate Activation with FeS (Mackinawite) and the Role of Sulfur Species in the Generation of Sulfate Radicals. *Chem. Eng. J.* **2021**, *407*, 126738. [CrossRef]
65. Zhang, P.; Zhang, X.; Zhao, X.; Jing, G.; Zhou, Z. Activation of Peracetic Acid with Zero-Valent Iron for Tetracycline Abatement: The Role of Fe(II) Complexation with Tetracycline. *J. Hazard. Mater.* **2022**, *424*, 127653. [CrossRef]
66. Li, L.; Wu, Y.; Dong, W. Enhancement in Sulfamethoxazole Degradation via Efficient Heterogeneous Activation of Peracetic Acid by FeS. *Water* **2024**, *16*, 2405. [CrossRef]
67. Joo, S.H.; Feitz, A.J.; Waite, T.D. Oxidative Degradation of the Carbothioate Herbicide, Molinate, Using Nanoscale Zero-Valent Iron. *Environ. Sci. Technol.* **2004**, *38*, 2242–2247. [CrossRef]
68. Noradoun, C.E.; Cheng, I.F. EDTA Degradation Induced by Oxygen Activation in a Zerovalent Iron/Air/Water System. *Environ. Sci. Technol.* **2005**, *39*, 7158–7163. [CrossRef]
69. Cheng, D.; Neumann, A.; Yuan, S.; Liao, W.; Qian, A. Oxidative Degradation of Organic Contaminants by FeS in the Presence of O_2. *Environ. Sci. Technol.* **2020**, *54*, 4091–4101. [CrossRef]
70. Pham, H.T.; Kitsuneduka, M.; Hara, J.; Suto, K.; Inoue, C. Trichloroethylene Transformation by Natural Mineral Pyrite: The Deciding Role of Oxygen. *Environ. Sci. Technol.* **2008**, *42*, 7470–7475. [CrossRef]
71. Ardo, S.G.; Nélieu, S.; Ona-Nguema, G.; Delarue, G.; Brest, J.; Pironin, E.; Morin, G. Oxidative Degradation of Nalidixic Acid by Nano-Magnetite via Fe^{2+}/O_2-Mediated Reactions. *Environ. Sci. Technol.* **2015**, *49*, 4506–4514. [CrossRef] [PubMed]
72. Chen, N.; Fang, G.; Liu, G.; Zhou, D.; Gao, J.; Gu, C. The Degradation of Diethyl Phthalate by Reduced Smectite Clays and Dissolved Oxygen. *Chem. Eng. J.* **2019**, *355*, 247–254. [CrossRef]
73. Pi, L.; Cai, J.; Xiong, L.; Cui, J.; Hua, H.; Tang, D.; Mao, X. Generation of H_2O_2 by On-Site Activation of Molecular Dioxygen for Environmental Remediation Applications: A Review. *Chem. Eng. J.* **2020**, *389*, 123420. [CrossRef]

74. Liu, Y.; Zhao, Y.; Wang, J. Fenton/Fenton-like Processes with in-Situ Production of Hydrogen Peroxide/Hydroxyl Radical for Degradation of Emerging Contaminants: Advances and Prospects. *J. Hazard. Mater.* **2021**, *404*, 124191. [CrossRef] [PubMed]
75. Li, Q.; Li, F. Recent Advances in Molecular Oxygen Activation via Photocatalysis and Its Application in Oxidation Reactions. *Chem. Eng. J.* **2021**, *421*, 129915. [CrossRef]
76. Ni, Y.; Zhou, C.; Xing, M.; Zhou, Y. Oxidation of Emerging Organic Contaminants by In-Situ H_2O_2 Fenton System. *Green Energy Environ.* **2024**, *9*, 417–434. [CrossRef]
77. Wilson, G.S. Determination of Oxidation-Reduction Potentials. *Methods Enzymol.* **1978**, *54*, 396–410.
78. Petersen, E.J.; Pinto, R.A.; Shi, X.; Huang, Q. Impact of Size and Sorption on Degradation of Trichloroethylene and Polychlorinated Biphenyls by Nano-Scale Zerovalent Iron. *J. Hazard. Mater.* **2012**, *243*, 73–79. [CrossRef]
79. Li, Q.; Yin, J.; Wu, L.; Li, S.; Chen, L. Effects of Biochar and Zero Valent Iron on the Bioavailability and Potential Toxicity of Heavy Metals in Contaminated Soil at the Field Scale. *Sci. Total Environ.* **2023**, *897*, 165386. [CrossRef]
80. Wei, K.; Li, H.; Gu, H.; Liu, X.; Ling, C.; Cao, S.; Li, M.; Liao, M.; Peng, X.; Shi, Y.; et al. Strained Zero-Valent Iron for Highly Efficient Heavy Metal Removal. *Adv. Funct. Mater.* **2022**, *32*, 2200498. [CrossRef]
81. Li, Y.; Kawashima, N.; Li, J.; Chandra, A.P.; Gerson, A.R. A Review of the Structure, and Fundamental Mechanisms and Kinetics of the Leaching of Chalcopyrite. *Adv. Colloid Interface Sci.* **2013**, *197–198*, 1–32. [CrossRef] [PubMed]
82. Zeng, Q.; Dong, H.; Wang, X. Effect of Ligands on the Production of Oxidants from Oxygenation of Reduced Fe-Bearing Clay Mineral Nontronite. *Geochim. Cosmochim. Acta* **2019**, *251*, 136–156. [CrossRef]
83. Zhang, Y.; Zhou, M. A Critical Review of the Application of Chelating Agents to Enable Fenton and Fenton-like Reactions at High pH Values. *J. Hazard. Mater.* **2019**, *362*, 436–450. [CrossRef] [PubMed]
84. Wang, Y.; Liu, L.; Fang, G.; Wang, L.; Kengara, F.O.; Zhu, C. The Mechanism of 2-Chlorobiphenyl Oxidative Degradation by Nanoscale Zero-Valent Iron in the Presence of Dissolved Oxygen. *Environ. Sci. Pollut. Res.* **2018**, *25*, 2265–2272. [CrossRef]
85. Wu, J.; Zhao, J.; Hou, J.; Zeng, R.J.; Xing, B. Degradation of Tetrabromobisphenol A by Sulfidated Nanoscale Zerovalent Iron in a Dynamic Two-Step Anoxic/Oxic Process. *Environ. Sci. Technol.* **2019**, *53*, 8105–8114. [CrossRef]
86. Keenan, C.R.; Sedlak, D.L. Factors Affecting the Yield of Oxidants from the Reaction of Nanoparticulate Zero-Valent Iron and Oxygen. *Environ. Sci. Technol.* **2008**, *42*, 1262–1267. [CrossRef]
87. Harada, T.; Yatagai, T.; Kawase, Y. Hydroxyl Radical Generation Linked with Iron Dissolution and Dissolved Oxygen Consumption in Zero-Valent Iron Wastewater Treatment Process. *Chem. Eng. J.* **2016**, *303*, 611–620. [CrossRef]
88. Lee, C.; Sedlak, D.L. Enhanced Formation of Oxidants from Bimetallic Nickel−Iron Nanoparticles in the Presence of Oxygen. *Environ. Sci. Technol.* **2008**, *42*, 8528–8533. [CrossRef]
89. Ai, Z.; Gao, Z.; Zhang, L.; He, W.; Yin, J.J. Core–Shell Structure Dependent Reactivity of Fe@Fe_2O_3 Nanowires on Aerobic Degradation of 4-Chlorophenol. *Environ. Sci. Technol.* **2013**, *47*, 5344–5352. [CrossRef]
90. He, D.; Ma, J.; Collins, R.N.; Waite, T.D. Effect of Structural Transformation of Nanoparticulate Zero-Valent Iron on Generation of Reactive Oxygen Species. *Environ. Sci. Technol.* **2016**, *50*, 3820–3828. [CrossRef]
91. Liu, X.; Fan, J.H.; Ma, L.M. Elimination of 4-Chlorophenol in Aqueous Solution by the Bimetallic Al–Fe/O_2 at Normal Temperature and Pressure. *Chem. Eng. J.* **2014**, *236*, 274–284. [CrossRef]
92. Fan, J.; Qin, H.; Zhang, Y.; Jiang, S. Degradation of 4-chlorophenol by BM Fe/Cu-O_2 System: The Symbiosis of and •OH Radicals. *Water Environ. Res.* **2019**, *91*, 770–779. [CrossRef] [PubMed]
93. Xiang, W.; Huang, M.; Wang, Y.; Wu, X.; Zhang, F.; Li, D.; Zhou, T. New Insight in the O_2 Activation by Nano Fe/Cu Bimetals: The Synergistic Role of Cu(0) and Fe(II). *Chin. Chem. Lett.* **2020**, *31*, 2831–2834. [CrossRef]
94. Yang, Z.; Zhang, X.; Pu, S.; Ni, R.; Lin, Y.; Liu, Y. Novel Fenton-like System (Mg/Fe-O_2) for Degradation of 4-Chlorophenol. *Environ. Pollut.* **2019**, *250*, 906–913. [CrossRef]
95. Wu, J.; Lin, M.; Liu, M.; Chen, Z. Novel Crystalline/Amorphous Heterophase Fe-Mn Core–Shell Chains on-Site Generate Hydrogen Peroxide in Aqueous Solution. *J. Colloid Interface Sci.* **2024**, *676*, 227–237. [CrossRef] [PubMed]
96. Tang, J.; Tang, L.; Feng, H.; Zeng, G.; Dong, H.; Zhang, C.; Huang, B.; Deng, Y.; Wang, J.; Zhou, Y. pH-Dependent Degradation of p-Nitrophenol by Sulfidated Nanoscale Zerovalent Iron under Aerobic or Anoxic Conditions. *J. Hazard. Mater.* **2016**, *320*, 581–590. [CrossRef] [PubMed]
97. Zhang, X.; Sun, W.; Wang, Y.; Li, Z.; Huang, X.; Li, T.; Wang, H. Mechanochemical Synthesis of Microscale Zero-Valent Iron/N-Doped Graphene-like Biochar Composite for Degradation of Tetracycline via Molecular O_2 Activation. *J. Colloid Interface Sci.* **2024**, *659*, 1015–1028. [CrossRef] [PubMed]
98. Yang, Y.; Xu, L.; Li, W.; Fan, W.; Song, S.; Yang, J. Adsorption and Degradation of Sulfadiazine over Nanoscale Zero-Valent Iron Encapsulated in Three-Dimensional Graphene Network through Oxygen-Driven Heterogeneous Fenton-like Reactions. *Appl. Catal. B* **2019**, *259*, 118057. [CrossRef]
99. Luo, Y.; Li, H.; Yang, H.; Yang, Z.; Li, C.; Liu, S.; Chen, Q.; Xu, W.; Zhang, W.; Tan, X. Critical Role of Dissolved Oxygen and Iron–Copper Synergy in Dual-Metal/Char Catalyst Systems. *Environ. Sci. Nano* **2024**, *11*, 2091–2102. [CrossRef]
100. Duan, L.; Liu, X.; Zhang, H.; Liu, F.; Liu, X.; Zhang, X.; Dong, L. A Novel Way for Hydroxyl Radicals Generation: Biochar-Supported Zero-Valent Iron Composite Activates Oxygen to Generate Hydroxyl Radicals. *J. Environ. Chem. Eng.* **2022**, *10*, 108132. [CrossRef]
101. Liu, Y.; Fan, Q.; Wang, J. Zn-Fe-CNTs Catalytic in Situ Generation of H_2O_2 for Fenton-like Degradation of Sulfamethoxazole. *J. Hazard. Mater.* **2018**, *342*, 166–176. [CrossRef] [PubMed]

102. Liu, Y.; Fan, Q.; Liu, Y.; Wang, J. Fenton-like Oxidation of 4-Chlorophenol Using H_2O_2 in Situ Generated by Zn-Fe-CNTs Composite. *J. Environ. Manag.* **2018**, *214*, 252–260. [CrossRef] [PubMed]
103. Lu, H.; Wen, C.; Gao, S.; Dong, Y.; Zhang, M.; Li, B.; Hu, W.; Dong, J. Incorporation of Nanoscale Zero-Valent Iron Particles in Monodisperse Mesoporous Silica Nanospheres: Characterization, Reactivity, Transport in Porous Media. *Colloids Surf. A* **2018**, *553*, 28–34. [CrossRef]
104. Yamaguchi, R.; Kurosu, S.; Suzuki, M.; Kawase, Y. Hydroxyl Radical Generation by Zero-Valent Iron/Cu (ZVI/Cu) Bimetallic Catalyst in Wastewater Treatment: Heterogeneous Fenton/Fenton-like Reactions by Fenton Reagents Formed in-Situ under Oxic Conditions. *Chem. Eng. J.* **2018**, *334*, 1537–1549. [CrossRef]
105. Chen, X.; Su, J.; Meng, Y.; Yu, M.; Zheng, M.; Sun, Y.; Xi, B. Oxygen Vacancy Promoted Heterogeneous Fenton-like Degradation of Sulfamethazine by Chlorine-Incorporated Micro Zero-Valent Iron. *Chem. Eng. J.* **2023**, *463*, 142360. [CrossRef]
106. Rajajayavel, S.R.C.; Ghoshal, S. Enhanced Reductive Dechlorination of Trichloroethylene by Sulfidated Nanoscale Zerovalent Iron. *Water Res.* **2015**, *78*, 144–153. [CrossRef]
107. Li, J.; Zhang, X.; Sun, Y.; Liang, L.; Pan, B.; Zhang, W.; Guan, X. Advances in Sulfidation of Zerovalent Iron for Water Decontamination. *Environ. Sci. Technol.* **2017**, *51*, 13533–13544. [CrossRef]
108. Xu, J.; Li, H.; Lowry, G.V. Sulfidized Nanoscale Zero-Valent Iron: Tuning the Properties of This Complex Material for Efficient Groundwater Remediation. *Acc. Mater. Res.* **2021**, *2*, 420–431. [CrossRef]
109. Garcia, A.N.; Zhang, Y.; Ghoshal, S.; He, F.; O'Carroll, D.M. Recent Advances in Sulfidated Zerovalent Iron for Contaminant Transformation. *Environ. Sci. Technol.* **2021**, *55*, 8464–8483. [CrossRef]
110. Song, S.; Su, Y.; Adeleye, A.S.; Zhang, Y.; Zhou, X. Optimal Design and Characterization of Sulfide-Modified Nanoscale Zerovalent Iron for Diclofenac Removal. *Appl. Catal. B* **2017**, *201*, 211–220. [CrossRef]
111. Ma, D.; Jia, S.; Zhao, D.; Lu, Z.; Yang, Z. O_2 Activation on the Outer Surface of Carbon Nanotubes Modified by Encapsulated Iron Clusters. *Appl. Surf. Sci.* **2014**, *300*, 91–97. [CrossRef]
112. Wang, B.; Zhou, X.; Wang, D.; Yin, J.-J.; Chen, H.; Gao, X.; Zhang, J.; Ibrahim, K.; Chai, Z.; Feng, W.; et al. Structure and Catalytic Activities of Ferrous Centers Confined on the Interface between Carbon Nanotubes and Humic Acid. *Nanoscale* **2015**, *7*, 2651–2658. [CrossRef] [PubMed]
113. Zhang, C.; Wang, D.; Liu, Q.; Tang, J. Ligand-Citric Acid Enhanced in-Situ ROS Generation by GBC@nZVI to Promote the Aerobic Degradation of Adsorbed 2,4-Dichlorophenol. *Chem. Eng. J.* **2023**, *477*, 147126. [CrossRef]
114. Rickard, D.; Luther, G.W. Chemistry of Iron Sulfides. *Chem. Rev.* **2007**, *107*, 514–562. [CrossRef] [PubMed]
115. Borda, M.J.; Elsetinow, A.R.; Schoonen, M.A.; Strongin, D.R. Pyrite-Induced Hydrogen Peroxide Formation as a Driving Force in the Evolution of Photosynthetic Organisms on an Early Earth. *Astrobiology* **2001**, *1*, 283–288. [CrossRef]
116. Nesbitt, H.W.; Bancroft, G.M.; Pratt, A.R.; Scaini, M.J. Sulfur and Iron Surface States on Fractured Pyrite Surfaces. *Am. Mineral.* **1998**, *83*, 1067–1076. [CrossRef]
117. Borda, M.J.; Elsetinow, A.R.; Strongin, D.R.; Schoonen, M.A. A Mechanism for the Production of Hydroxyl Radical at Surface Defect Sites on Pyrite. *Geochim. Cosmochim. Acta* **2003**, *67*, 935–939. [CrossRef]
118. Ling, C.; Liu, X.; Li, M.; Wang, X.; Shi, Y.; Qi, J.; Zhao, J.; Zhang, L. Sulphur Vacancy Derived Anaerobic Hydroxyl Radical Generation at the Pyrite-Water Interface: Pollutants Removal and Pyrite Self-Oxidation Behavior. *Appl. Catal. B* **2021**, *290*, 120051. [CrossRef]
119. Zhang, P.; Yuan, S.; Liao, P. Mechanisms of Hydroxyl Radical Production from Abiotic Oxidation of Pyrite under Acidic Conditions. *Geochim. Cosmochim. Acta* **2016**, *172*, 444–457. [CrossRef]
120. Hao, F.; Guo, W.; Lin, X.; Leng, Y.; Wang, A.; Yue, X.; Yan, L. Degradation of Acid Orange 7 in Aqueous Solution by Dioxygen Activation in a Pyrite/H_2O/O_2 System. *Environ. Sci. Pollut. Res.* **2014**, *21*, 6723–6728. [CrossRef]
121. Tan, M.; Zheng, X.; Yu, W.; Chen, B.; Chu, C. Facet-Dependent Productions of Reactive Oxygen Species from Pyrite Oxidation. *Environ. Sci. Technol.* **2024**, *58*, 432–439. [CrossRef] [PubMed]
122. Zhu, L.; Wang, H.; Sun, J.; Lu, L.; Li, S. Sulfur Vacancies in Pyrite Trigger the Path to Nonradical Singlet Oxygen and Spontaneous Sulfamethoxazole Degradation: Unveiling the Hidden Potential in Sediments. *Environ. Sci. Technol.* **2024**, *58*, 6753–6762. [CrossRef] [PubMed]
123. Gao, X.; Dai, C.; Tian, X.; Nie, Y.; Shi, J. Self-Acclimation Mechanism of Pyrite to Sulfamethoxazole Concentration in Terms of Degradation Behavior and Toxicity Effects Caused by Reactive Oxygen Species. *J. Hazard. Mater.* **2024**, *464*, 132962. [CrossRef] [PubMed]
124. Chen, X.; Xian, Z.; Gao, S.; Bai, L.; Liang, S.; Tian, H.; Wang, C.; Gu, C. Mechanistic Insights into Surface Catalytic Oxidation of Fluoroquinolone Antibiotics on Sediment Mackinawite. *Water Res.* **2023**, *232*, 119651. [CrossRef]
125. Cheng, D.; Liao, W.; Yuan, S. Effect of in Situ Generated Iron Oxyhydroxide Coatings on FeS Oxygenation and Resultant Hydroxyl Radical Production for Contaminant Degradation. *Chem. Eng. J.* **2020**, *394*, 124961. [CrossRef]
126. Cohn, C.A.; Mueller, S.; Wimmer, E.; Leifer, N.; Greenbaum, S.; Strongin, D.R.; Schoonen, M.A. Pyrite-Induced Hydroxyl Radical Formation and Its Effect on Nucleic Acids. *Geochem. Trans.* **2006**, *7*, 3. [CrossRef]
127. Kong, L.; Hu, X.; He, M. Mechanisms of Sb(III) Oxidation by Pyrite-Induced Hydroxyl Radicals and Hydrogen Peroxide. *Environ. Sci. Technol.* **2015**, *49*, 3499–3505. [CrossRef]
128. Song, B.; Zeng, Z.; Almatrafi, E.; Shen, M.; Xiong, W.; Zhou, C.; Wang, W.; Zeng, G.; Gong, J. Pyrite-Mediated Advanced Oxidation Processes: Applications, Mechanisms, and Enhancing Strategies. *Water Res.* **2022**, *211*, 118048. [CrossRef]

129. Schoonen, M.A.A.; Cohn, C.A.; Roemer, E.; Laffers, R.; Simon, S.R.; O'Riordan, T. Mineral-Induced Formation of Reactive Oxygen Species. *Rev. Mineral. Geochem.* **2006**, *64*, 179–221. [CrossRef]
130. Fan, D.; Lan, Y.; Tratnyek, P.G.; Johnson, R.L.; Filip, J.; O'Carroll, D.M.; Nunez Garcia, A.; Agrawal, A. Sulfidation of Iron-Based Materials: A Review of Processes and Implications for Water Treatment and Remediation. *Environ. Sci. Technol.* **2017**, *51*, 13070–13085. [CrossRef]
131. Dos Santos, E.C.; de Mendonça Silva, J.C.; Duarte, H.A. Pyrite Oxidation Mechanism by Oxygen in Aqueous Medium. *J. Phys. Chem. C* **2016**, *120*, 2760–2768. [CrossRef]
132. Usher, C.R.; Cleveland, C.A.; Strongin, D.R.; Schoonen, M.A. Origin of Oxygen in Sulfate during Pyrite Oxidation with Water and Dissolved Oxygen: An In Situ Horizontal Attenuated Total Reflectance Infrared Spectroscopy Isotope Study. *Environ. Sci. Technol.* **2004**, *38*, 5604–5606. [CrossRef] [PubMed]
133. Tang, B.; Liang, J.; Wen, Z.; Zhou, Y.; Yan, Z.; Zhou, Y.; He, P.; Gu, C.; Gan, M.; Zhu, J. Insight into the Crystal Facet-Dependent Cr(VI) Reduction: A Comparative Study of Pyrite {100} and {111} Facets. *J. Environ. Sci.* **2025**, *150*, 78–79. [CrossRef] [PubMed]
134. Zhou, S.; Gan, M.; Wang, X.; Zhang, Y.; Fang, Y.; Gu, G.; Wang, Y.; Qiu, G. ROS Formation Driven by Pyrite-Mediated Arsenopyrite Oxidation and Its Potential Role on Arsenic Transformation. *J. Hazard. Mater.* **2023**, *443*, 130151. [CrossRef] [PubMed]
135. Wehrli, B.; Sulzberger, B.; Stumm, W. Redox Processes Catalyzed by Hydrous Oxide Surfaces. *Chem. Geol.* **1989**, *78*, 167–179. [CrossRef]
136. Schoonen, M.A.A.; Harrington, A.D.; Laffers, R.; Strongin, D.R. Role of Hydrogen Peroxide and Hydroxyl Radical in Pyrite Oxidation by Molecular Oxygen. *Geochim. Cosmochim. Acta* **2010**, *74*, 4971–4987. [CrossRef]
137. Nicholson, R.V.; Gillham, R.W.; Reardon, E.J. Pyrite Oxidation in Carbonate-Buffered Solution: 2. Rate Control by Oxide Coatings. *Geochim. Cosmochim. Acta* **1990**, *54*, 395–402. [CrossRef]
138. Liu, R.; Dai, Y.; Feng, Y.; Sun, S.; Zhang, X.; An, C.; Zhao, S. Hydroxyl Radical Production by Abiotic Oxidation of Pyrite under Estuarine Conditions: The Effects of Aging, Seawater Anions and Illumination. *J. Environ. Sci.* **2024**, *135*, 715–727. [CrossRef]
139. Morgan, B.; Rate, A.W.; Burton, E.D. Water Chemistry and Nutrient Release during the Resuspension of FeS-Rich Sediments in a Eutrophic Estuarine System. *Sci. Total Environ.* **2012**, *432*, 47–56. [CrossRef]
140. Jeong, H.Y.; Han, Y.-S.; Park, S.W.; Hayes, K.F. Aerobic Oxidation of Mackinawite (FeS) and Its Environmental Implication for Arsenic Mobilization. *Geochim. Cosmochim. Acta* **2010**, *74*, 3182–3198. [CrossRef]
141. Jeong, H.Y.; Han, Y.-S.; Hayes, K.F. X-Ray Absorption and X-Ray Photoelectron Spectroscopic Study of Arsenic Mobilization during Mackinawite (FeS) Oxidation. *Environ. Sci. Technol.* **2010**, *44*, 955–961. [CrossRef] [PubMed]
142. Bi, Y.; Stylo, M.; Bernier-Latmani, R.; Hayes, K.F. Rapid Mobilization of Noncrystalline U(IV) Coupled with FeS Oxidation. *Environ. Sci. Technol.* **2016**, *50*, 1403–1411. [CrossRef] [PubMed]
143. Cheng, D.; Yuan, S.; Liao, P.; Zhang, P. Oxidizing Impact Induced by Mackinawite (FeS) Nanoparticles at Oxic Conditions Due to Production of Hydroxyl Radicals. *Environ. Sci. Technol.* **2016**, *50*, 11646–11653. [CrossRef] [PubMed]
144. Zhu, A.; Guo, Y.; Liu, G.; Song, M.; Liang, Y.; Cai, Y.; Yin, Y. Hydroxyl Radical Formation upon Dark Oxidation of Reduced Iron Minerals: Effects of Iron Species and Environmental Factors. *Chin. Chem. Lett.* **2019**, *30*, 2241–2244. [CrossRef]
145. Chiriţă, P.; Schlegel, M.L. Oxidative Dissolution of Iron Monosulfide (FeS) in Acidic Conditions: The Effect of Solid Pretreatment. *Int. J. Miner. Process.* **2015**, *135*, 57–64. [CrossRef]
146. Xiao, H.; Wang, Y.; Peng, H.; Zhu, Y.; Fang, D.; Wu, G.; Li, L.; Zeng, Z. Highly Efficient Degradation of Tetracycline Hydrochloride in Water by Oxygenation of Carboxymethyl Cellulose-Stabilized FeS Nanofluids. *Int. J. Environ. Res. Public Health* **2022**, *19*, 11447. [CrossRef]
147. He, J.; Miller, C.J.; Collins, R.; Wang, D.; Waite, T.D. Production of a Surface-Localized Oxidant during Oxygenation of Mackinawite (FeS). *Environ. Sci. Technol.* **2020**, *54*, 1167–1176. [CrossRef]
148. Meng, F.; Tong, H.; Feng, C.; Huang, Z.; Wu, P.; Zhou, J.; Hua, J.; Wu, F.; Liu, C. Structural Fe(II)-Induced Generation of Reactive Oxygen Species on Magnetite Surface for Aqueous As(III) Oxidation during Oxygen Activation. *Water Res.* **2024**, *252*, 121232. [CrossRef]
149. Fang, G.D.; Zhou, D.M.; Dionysiou, D.D. Superoxide Mediated Production of Hydroxyl Radicals by Magnetite Nanoparticles: Demonstration in the Degradation of 2-Chlorobiphenyl. *J. Hazard. Mater.* **2013**, *250–251*, 68–75. [CrossRef]
150. Fang, L.; Gao, B.; Li, F.; Liu, K.; Chi, J. The Nature of Metal Atoms Incorporated in Hematite Determines Oxygen Activation by Surface-Bound Fe(II) for As(III) Oxidation. *Water Res.* **2022**, *227*, 119351. [CrossRef]
151. Ding, Y.; Ruan, Y.; Zhu, L.; Tang, H. Efficient Oxidative Degradation of Chlorophenols by Using Magnetic Surface Carboxylated Cu^0/Fe_3O_4 Nanocomposites in a Wide pH Range. *J. Environ. Chem. Eng.* **2017**, *5*, 2681–2690. [CrossRef]
152. Yang, Z.; Gong, X.; Peng, L.; Yang, D.; Liu, Y. Zn^0-CNTs-Fe_3O_4 Catalytic in Situ Generation of H_2O_2 for Heterogeneous Fenton Degradation of 4-Chlorophenol. *Chemosphere* **2018**, *208*, 665–673. [CrossRef] [PubMed]
153. Wu, Y.; Tan, X.; Wang, E.; Zhao, J.; Ma, J. A Facile Strategy to Convert Low-Activity Commercial Iron Oxides and Cobalt Disulfide into High-Activity Fenton-like Catalysts: Spontaneous Generation of $^1O_2$ for Aqueous Decontamination. *Mater. Today Chem.* **2022**, *26*, 101106. [CrossRef]
154. Zhang, P.; Zhang, W.; Yu, H.; Chen, R.; Liu, Y.; Tian, Y.; Yuan, S. Fe(III) Oxyhydroxides Mediated Electron Transfer from Thiols to O_2 for Hydroxyl Radical Production. *Chem. Geol.* **2024**, *648*, 121962. [CrossRef]

155. Li, D.; Sun, J.; Fu, Y.; Hong, W.; Wang, H.; Yang, Q.; Wu, J.; Yang, S.; Xu, J.; Zhang, Y.; et al. Fluctuating Redox Conditions Accelerate the Electron Storage and Transfer in Magnetite and Production of Dark Hydroxyl Radicals. *Water Res.* **2024**, *248*, 120884. [CrossRef]
156. Hong, Z.; Li, F.; Borch, T.; Shi, Q.; Fang, L. Incorporation of Cu into Goethite Stimulates Oxygen Activation by Surface-Bound Fe(II) for Enhanced As(III) Oxidative Transformation. *Environ. Sci. Technol.* **2023**, *57*, 2162–2174. [CrossRef]
157. Amstaetter, K.; Borch, T.; Larese-Casanova, P.; Kappler, A. Redox Transformation of Arsenic by Fe(II)-Activated Goethite (α-FeOOH). *Environ. Sci. Technol.* **2010**, *44*, 102–108. [CrossRef]
158. Warr, L.N. Earth's Clay Mineral Inventory and Its Climate Interaction: A Quantitative Assessment. *Earth-Sci. Rev.* **2022**, *234*, 104198. [CrossRef]
159. Yuan, S.; Liu, X.; Liao, W.; Zhang, P.; Wang, X.; Tong, M. Mechanisms of Electron Transfer from Structrual Fe(II) in Reduced Nontronite to Oxygen for Production of Hydroxyl Radicals. *Geochim. Cosmochim. Acta* **2018**, *223*, 422–436. [CrossRef]
160. Liu, X.; Yuan, S.; Tong, M.; Liu, D. Oxidation of Trichloroethylene by the Hydroxyl Radicals Produced from Oxygenation of Reduced Nontronite. *Water Res.* **2017**, *113*, 72–79. [CrossRef]
161. Zeng, Q.; Dong, H.; Wang, X.; Yu, T.; Cui, W. Degradation of 1,4-Dioxane by Hydroxyl Radicals Produced from Clay Minerals. *J. Hazard. Mater.* **2017**, *331*, 88–98. [CrossRef] [PubMed]
162. Guo, J.; Zhang, X. The Impact of Electron Transfer between Structural Fe(II) and Aqueous Fe(III) on the Redox Transformation of Arsenic. *Environ. Earth Sci.* **2023**, *82*, 304. [CrossRef]
163. Yu, C.; Qian, A.; Lu, Y.; Liao, W.; Zhang, P.; Tong, M.; Dong, H.; Zeng, Q.; Yuan, S. Electron Transfer Processes Associated with Structural Fe in Clay Minerals. *Crit. Rev. Environ. Sci. Technol.* **2024**, *54*, 13–38. [CrossRef]
164. Zhang, P.; Liu, J.; Yu, H.; Cheng, D.; Liu, H.; Yuan, S. Kinetic Models for Hydroxyl Radical Production and Contaminant Removal during Soil/Sediment Oxygenation. *Water Res.* **2023**, *240*, 120071. [CrossRef]
165. Yu, C.; Ji, W.; Li, X.; Yuan, S.; Zhang, P.; Pu, S. Critical Role of Mineral Fe(IV) Formation in Low Hydroxyl Radical Yields during Fe(II)-Bearing Clay Mineral Oxygenation. *Environ. Sci. Technol.* **2024**, *58*, 9669–9678. [CrossRef]
166. Rothwell, K.A.; Pentrak, M.P.; Pentrak, L.A.; Stucki, J.W.; Neumann, A. Reduction Pathway-Dependent Formation of Reactive Fe(II) Sites in Clay Minerals. *Environ. Sci. Technol.* **2023**, *57*, 10231–10241. [CrossRef]
167. Zhao, G.; Tan, M.; Wu, B.; Zheng, X.; Xiong, R.; Chen, B.; Kappler, A.; Chu, C. Redox Oscillations Activate Thermodynamically Stable Iron Minerals for Enhanced Reactive Oxygen Species Production. *Environ. Sci. Technol.* **2023**, *57*, 8628–8637. [CrossRef]
168. Xie, W.; Yuan, S.; Tong, M.; Ma, S.; Liao, W.; Zhang, N.; Chen, C. Contaminant Degradation by •OH during Sediment Oxygenation: Dependence on Fe(II) Species. *Environ. Sci. Technol.* **2020**, *54*, 2975–2984. [CrossRef]
169. Chen, N.; Huang, D.; Liu, G.; Chu, L.; Fang, G.; Zhu, C.; Zhou, D.; Gao, J. Active Iron Species Driven Hydroxyl Radicals Formation in Oxygenation of Different Paddy Soils: Implications to Polycyclic Aromatic Hydrocarbons Degradation. *Water Res.* **2021**, *203*, 117484. [CrossRef]
170. Liu, J.; Zhu, C.; Zhu, F.; Sun, H.; Wang, J.; Fang, G.; Zhou, D. Strong Substance Exchange at Paddy Soil-Water Interface Promotes Nonphotochemical Formation of Reactive Oxygen Species in Overlying Water. *Environ. Sci. Technol.* **2024**, *58*, 7403–7414. [CrossRef]
171. Huang, D.; Chen, N.; Zhu, C.; Sun, H.; Fang, G.; Zhou, D. Dynamic Production of Hydroxyl Radicals during the Flooding–Drainage Process of Paddy Soil: An In Situ Column Study. *Environ. Sci. Technol.* **2023**, *57*, 16340–16347. [CrossRef] [PubMed]
172. Feng, Y.; Dai, Y.; Liu, R.; Zhao, D.; Sun, S.; Xu, X.; Chen, Y.; Yuan, X.; Zhang, B.; Zhao, S. Production and Prediction of Hydroxyl Radicals in Distinct Redox-Fluctuation Zones of the Yellow River Estuary. *J. Hazard. Mater.* **2024**, *469*, 133980. [CrossRef] [PubMed]
173. Liu, F.; Wang, Z.; Liu, J.; Latif, J.; Qin, J.; Yang, H.; Jiang, W.; Deng, Y.; Yang, K.; Ni, Z.; et al. Seasonal and Spatial Fluctuations of Reactive Oxygen Species in Riparian Soils and Their Contributions on Organic Carbon Mineralization. *Environ. Sci. Technol.* **2024**, *58*, 7066–7077. [CrossRef] [PubMed]
174. Zhao, G.; Wu, B.; Zheng, X.; Chen, B.; Kappler, A.; Chu, C. Tide-Triggered Production of Reactive Oxygen Species in Coastal Soils. *Environ. Sci. Technol.* **2022**, *56*, 11888–11896. [CrossRef]
175. Chen, N.; Fu, Q.; Wu, T.; Cui, P.; Fang, G.; Liu, C.; Chen, C.; Liu, G.; Wang, W.; Wang, D.; et al. Active Iron Phases Regulate the Abiotic Transformation of Organic Carbon during Redox Fluctuation Cycles of Paddy Soil. *Environ. Sci. Technol.* **2021**, *55*, 14281–14293. [CrossRef]
176. Lu, J.; Yu, P.; Zhang, J.; Guo, Z.; Li, Y.; Wang, S.; Hu, Z. Biotic/Abiotic Transformation Mechanisms of Phenanthrene in Iron-Rich Constructed Wetland under Redox Fluctuation. *Water Res.* **2024**, *261*, 122033. [CrossRef]
177. Sun, Z.; Huang, M.; Liu, C.; Fang, G.; Chen, N.; Zhou, D.; Gao, J. The Formation of •OH with Fe-Bearing Smectite Clays and Low-Molecular-Weight Thiols: Implication of As(III) Removal. *Water Res.* **2020**, *174*, 115631. [CrossRef]
178. Schaefer, C.E.; Ho, P.; Berns, E.; Werth, C. Mechanisms for Abiotic Dechlorination of Trichloroethene by Ferrous Minerals under Oxic and Anoxic Conditions in Natural Sediments. *Environ. Sci. Technol.* **2018**, *52*, 13747–13755. [CrossRef]
179. Kasozi, N.; Tandlich, R.; Fick, M.; Kaiser, H.; Wilhelmi, B. Iron Supplementation and Management in Aquaponic Systems: A Review. *Aquac. Rep.* **2019**, *15*, 100221. [CrossRef]
180. Ren, H.; He, F.; Liu, S.; Li, T.; Zhou, R. Enhancing Fenton–like Process at Neutral pH by Fe(III)–GLDA Complexation for the Oxidation Removal of Organic Pollutants. *J. Hazard. Mater.* **2021**, *416*, 126077. [CrossRef]
181. Jones, A.M.; Griffin, P.J.; Waite, T.D. Ferrous Iron Oxidation by Molecular Oxygen under Acidic Conditions: The Effect of Citrate, EDTA and Fulvic Acid. *Geochim. Cosmochim. Acta* **2015**, *160*, 117–131. [CrossRef]

182. Zhang, P.; Yuan, S. Production of Hydroxyl Radicals from Abiotic Oxidation of Pyrite by Oxygen under Circumneutral Conditions in the Presence of Low-Molecular-Weight Organic Acids. *Geochim. Cosmochim. Acta* **2017**, *218*, 153–166. [CrossRef]
183. Wang, Y.; Kong, L.; He, M.; Lin, C.; Ouyang, W.; Liu, X.; Peng, X. Mechanistic Insights into Sb(III) and Fe(II) Co-Oxidation by Oxygen and Hydrogen Peroxide: Dominant Reactive Oxygen Species and Roles of Organic Ligands. *Water Res.* **2023**, *242*, 120296. [CrossRef] [PubMed]
184. Wang, Q.; Pan, Y.; Fu, W.; Wu, H.; Zhou, M.; Zhang, Y. Aminopolycarboxylic Acids Modified Oxygen Reduction by Zero Valent Iron: Proton-Coupled Electron Transfer, Role of Iron Ion and Reactive Oxidant Generation. *J. Hazard. Mater.* **2022**, *430*, 128402. [CrossRef] [PubMed]
185. Checa-Fernandez, A.; Santos, A.; Romero, A.; Dominguez, C.M. Application of Chelating Agents to Enhance Fenton Process in Soil Remediation: A Review. *Catalysts* **2021**, *11*, 722. [CrossRef]
186. De Laat, J.; Dao, Y.H.; Hamdi El Najjar, N.; Daou, C. Effect of Some Parameters on the Rate of the Catalysed Decomposition of Hydrogen Peroxide by Iron(III)-Nitrilotriacetate in Water. *Water Res.* **2011**, *45*, 5654–5664. [CrossRef]
187. Zhang, Y.; Klamerth, N.; Messele, S.A.; Chelme-Ayala, P.; Gamal El-Din, M. Kinetics Study on the Degradation of a Model Naphthenic Acid by Ethylenediamine-N,N′-Disuccinic Acid-Modified Fenton Process. *J. Hazard. Mater.* **2016**, *318*, 371–378. [CrossRef]
188. Zhou, H.; Sun, Q.; Wang, X.; Wang, L.; Chen, J.; Zhang, J.; Lu, X. Removal of 2,4-Dichlorophenol from Contaminated Soil by a Heterogeneous ZVI/EDTA/Air Fenton-like System. *Sep. Purif. Technol.* **2014**, *132*, 346–353. [CrossRef]
189. Huang, M.; Fang, G.; Chen, N.; Zhou, D. Hydroxylamine Promoted Hydroxyl Radical Production and Organic Contaminants Degradation in Oxygenation of Pyrite. *J. Hazard. Mater.* **2022**, *429*, 128380. [CrossRef]
190. Li, K.; Ma, S.; Zou, C.; Latif, J.; Jiang, Y.; Ni, Z.; Shen, S.; Feng, J.; Jia, H. Unrecognized Role of Organic Acid in Natural Attenuation of Pollutants by Mackinawite (FeS): The Significance of Carbon-Center Free Radicals. *Environ. Sci. Technol.* **2023**, *57*, 20871–20880. [CrossRef]
191. Yu, C.; Zhang, Y.; Lu, Y.; Qian, A.; Zhang, P.; Cui, Y.; Yuan, S. Mechanistic Insight into Humic Acid-Enhanced Hydroxyl Radical Production from Fe(II)-Bearing Clay Mineral Oxygenation. *Environ. Sci. Technol.* **2021**, *55*, 13366–13375. [PubMed]
192. Cheng, D.; Ding, H.; Tan, Y.; Yang, D.; Pan, Y.; Liao, W.; He, F. Dramatically Enhanced Phenol Degradation upon FeS Oxygenation by Low-Molecular-Weight Organic Acids. *J. Hazard. Mater.* **2023**, *459*, 132260. [CrossRef] [PubMed]
193. Mohamad, N.D.; Zaki, Z.M.; Amir, A. Mechanisms of Enhanced Oxidative Degradation of Tetrachloroethene by Nano-Magnetite Catalysed with Glutathione. *Chem. Eng. J.* **2020**, *393*, 124760. [CrossRef]
194. Zhao, S.; Liu, Z.; Zhang, R.; Liu, J.; Liu, J.; Dai, Y.; Zhang, C.; Jia, H. Interfacial Reaction between Organic Acids and Iron-Containing Clay Minerals: Hydroxyl Radical Generation and Phenolic Compounds Degradation. *Sci. Total Environ.* **2021**, *783*, 147025. [CrossRef]
195. Qin, Y.; Song, F.; Ai, Z.; Zhang, P.; Zhang, L. Protocatechuic Acid Promoted Alachlor Degradation in Fe(III)/H_2O_2 Fenton System. *Environ. Sci. Technol.* **2015**, *49*, 7948–7956. [CrossRef]
196. Xie, L.; Shang, C. Role of Humic Acid and Quinone Model Compounds in Bromate Reduction by Zerovalent Iron. *Environ. Sci. Technol.* **2005**, *39*, 1092–1100. [CrossRef]
197. Liu, Z.; Fu, J.; Liu, A.; Zhang, W.-X. Influence of Natural Organic Matter on Nanoscale Zero-Valent Iron for Contaminants Removal in Water: A Critical Review. *Chem. Eng. J.* **2024**, *488*, 150836. [CrossRef]
198. Liu, Y.; Zhao, W.; Zhang, P.; Fu, Q.; Yu, C.; Yuan, S. Asymmetrical Changes of Electron-Donating and Electron-Accepting Capacities of Natural Organic Matter during Its Interaction with Fe Oxyhydroxides. *Chem. Geol.* **2024**, *661*, 122189. [CrossRef]
199. Dong, H.; Zeng, Q.; Sheng, Y.; Chen, C.; Yu, G.; Kappler, A. Coupled Iron Cycling and Organic Matter Transformation across Redox Interfaces. *Nat. Rev. Earth Environ.* **2023**, *4*, 659–673. [CrossRef]
200. Wolf, M.; Kappler, A.; Jiang, J.; Meckenstock, R.U. Effects of Humic Substances and Quinones at Low Concentrations on Ferrihydrite Reduction by *Geobacter Metallireducens*. *Environ. Sci. Technol.* **2009**, *43*, 5679–5685. [CrossRef]
201. Zeng, Q.; Wang, X.; Liu, X.; Huang, L.; Hu, J.; Chu, R.; Tolic, N.; Dong, H. Mutual Interactions between Reduced Fe-Bearing Clay Minerals and Humic Acids under Dark, Oxygenated Conditions: Hydroxyl Radical Generation and Humic Acid Transformation. *Environ. Sci. Technol.* **2020**, *54*, 15013–15023. [CrossRef] [PubMed]
202. Yuan, Y.; Wei, X.; Zhu, M.; Cai, Y.; Wang, Y.; Dang, Z.; Yin, H. Unravelling the Removal Mechanisms of Trivalent Arsenic by Sulfidated Nanoscale Zero-Valent Iron: The Crucial Role of Reactive Oxygen Species and the Multiple Effects of Citric Acid. *Sci. Total Environ.* **2024**, *916*, 170275. [CrossRef]
203. Cheng, X.; Liang, L.; Ye, J.; Li, N.; Yan, B.; Chen, G. Influence and Mechanism of Water Matrices on H_2O_2-Based Fenton-like Oxidation Processes: A Review. *Sci. Total Environ.* **2023**, *888*, 164086. [CrossRef] [PubMed]
204. Fang, L.; Xu, L.; Deng, J.; Gao, S.; Huang, L.Z. Induced Generation of Hydroxyl Radicals from Green Rust under Oxic Conditions by Iron-Phosphate Complexes. *Chem. Eng. J.* **2021**, *414*, 128780. [CrossRef]
205. Mu, Y.; Ai, Z.; Zhang, L. Phosphate Shifted Oxygen Reduction Pathway on Fe@Fe_2O_3 Core–Shell Nanowires for Enhanced Reactive Oxygen Species Generation and Aerobic 4-Chlorophenol Degradation. *Environ. Sci. Technol.* **2017**, *51*, 8101–8109. [CrossRef]
206. Wang, J.; Wang, S. Effect of Inorganic Anions on the Performance of Advanced Oxidation Processes for Degradation of Organic Contaminants. *Chem. Eng. J.* **2021**, *411*, 128392. [CrossRef]

207. Hug, S.J.; Leupin, O. Iron-Catalyzed Oxidation of Arsenic(III) by Oxygen and by Hydrogen Peroxide: pH-Dependent Formation of Oxidants in the Fenton Reaction. *Environ. Sci. Technol.* **2003**, *37*, 2734–2742. [CrossRef]
208. Ernstsen, V.; Gates, W.P.; Stucki, J.W. Microbial Reduction of Structural Iron in Clays—A Renewable Source of Reduction Capacity. *J. Environ. Qual.* **1998**, *27*, 761–766. [CrossRef]
209. Chen, R.; Liu, H.; Zhang, P.; Ma, J.; Jin, M. Co-Response of Fe-Reducing/Oxidizing Bacteria and Fe Species to the Dynamic Redox Cycles of Natural Sediment. *Sci. Total Environ.* **2022**, *815*, 152953. [CrossRef]
210. Han, R.; Lv, J.; Huang, Z.; Zhang, S.; Zhang, S. Pathway for the Production of Hydroxyl Radicals during the Microbially Mediated Redox Transformation of Iron (Oxyhydr)oxides. *Environ. Sci. Technol.* **2020**, *54*, 902–910. [CrossRef]
211. Dong, H.; Coffin, E.S.; Sheng, Y.; Duley, M.L.; Khalifa, Y.M. Microbial Reduction of Fe(III) in Nontronite: Role of Biochar as a Redox Mediator. *Geochim. Cosmochim. Acta* **2023**, *345*, 102–116. [CrossRef]
212. Pi, K.; Markelova, E.; Zhang, P.; Van Cappellen, P. Arsenic Oxidation by Flavin-Derived Reactive Species under Oxic and Anoxic Conditions: Oxidant Formation and pH Dependence. *Environ. Sci. Technol.* **2019**, *53*, 10897–10905. [CrossRef]
213. Dong, H.; Kukkadapu, R.K.; Fredrickson, J.K.; Zachara, J.M.; Kennedy, D.W.; Kostandarithes, H.M. Microbial Reduction of Structural Fe(III) in Illite and Goethite. *Environ. Sci. Technol.* **2003**, *37*, 1268–1276. [CrossRef]
214. You, X.; Liu, S.; Berns-Herrboldt, E.C.; Dai, C.; Werth, C.J. Kinetics of Hydroxyl Radical Production from Oxygenation of Reduced Iron Minerals and Their Reactivity with Trichloroethene: Effects of Iron Amounts, Iron Species, and Sulfate Reducing Bacteria. *Environ. Sci. Technol.* **2023**, *57*, 4892–4904. [CrossRef] [PubMed]
215. Edwards, K.J.; Bach, W.; McCollom, T.M.; Rogers, D.R. Neutrophilic Iron-Oxidizing Bacteria in the Ocean: Their Habitats, Diversity, and Roles in Mineral Deposition, Rock Alteration, and Biomass Production in the Deep-Sea. *Geomicrobiol. J.* **2004**, *21*, 393–404. [CrossRef]
216. Jones, S.; Santini, J.M. Mechanisms of Bioleaching: Iron and Sulfur Oxidation by Acidophilic Microorganisms. *Essays Biochem.* **2023**, *67*, 685–699.
217. Xie, Z.H.; He, C.S.; Pei, D.N.; Dong, Y.; Yang, S.R.; Xiong, Z.; Zhou, P.; Pan, Z.C.; Yao, G.; Lai, B. Review of Characteristics, Generation Pathways and Detection Methods of Singlet Oxygen Generated in Advanced Oxidation Processes (AOPs). *Chem. Eng. J.* **2023**, *468*, 143778. [CrossRef]
218. Sun, Y.; Han, W.; Zhang, F.; Li, H.; Zhang, Z.; Zhang, X.; Shen, B.; Guo, S.Q.; Ma, T. Dual Defect Regulation of BiOCl Halogen Layer Enables Photocatalytic O_2 Activation into Singlet Oxygen for Refractory Aromatic Pollutant Removal. *Appl. Catal. B* **2024**, *345*, 123689. [CrossRef]
219. Yu, W.; Zheng, X.; Tan, M.; Wang, J.; Wu, B.; Ma, J.; Pan, Y.; Chen, B.; Chu, C. Field Quantification of Hydroxyl Radicals by Flow-Injection Chemiluminescence Analysis with a Portable Device. *Environ. Sci. Technol.* **2024**, *58*, 2808–2816. [CrossRef]
220. Bai, L.; Jiang, Y.; Xia, D.; Wei, Z.; Spinney, R.; Dionysiou, D.D.; Minakata, D.; Xiao, R.; Xie, H.-B.; Chai, L. Mechanistic Understanding of Superoxide Radical-Mediated Degradation of Perfluorocarboxylic Acids. *Environ. Sci. Technol.* **2022**, *56*, 624–633. [CrossRef]
221. Wang, R.; Chen, H.; He, Z.; Zhang, S.; Wang, K.; Ren, N.; Ho, S.-H. Discovery of an End-to-End Pattern for Contaminant-Oriented Advanced Oxidation Processes Catalyzed by Biochar with Explainable Machine Learning. *Environ. Sci. Technol.* **2024**, *58*, 16867–16876. [CrossRef] [PubMed]
222. Cao, X.; Huang, J.; Tian, Y.; Hu, Z.; Luo, Z.; Wang, J.; Guo, Y. Machine-Learning-Assisted Descriptors Identification for Indoor Formaldehyde Oxidation Catalysts. *Environ. Sci. Technol.* **2024**, *58*, 8372–8379. [CrossRef] [PubMed]
223. Hjorth, R.; Coutris, C.; Nguyen, N.H.A.; Sevcu, A.; Gallego-Urrea, J.A.; Baun, A.; Joner, E.J. Ecotoxicity Testing and Environmental Risk Assessment of Iron Nanomaterials for Sub-Surface Remediation—Recommendations from the FP7 Project NanoRem. *Chemosphere* **2017**, *182*, 525–531. [CrossRef] [PubMed]
224. Zhang, S.; Yi, K.; Chen, A.; Shao, J.; Peng, L.; Luo, S. Toxicity of Zero-Valent Iron Nanoparticles to Soil Organisms and the Associated Defense Mechanisms: A Review. *Ecotoxicology* **2022**, *31*, 873–883. [CrossRef]
225. Zeng, G.; He, Y.; Wang, F.; Luo, H.; Liang, D.; Wang, J.; Huang, J.; Yu, C.; Jin, L.; Sun, D. Toxicity of Nanoscale Zero-Valent Iron to Soil Microorganisms and Related Defense Mechanisms: A Review. *Toxics* **2023**, *11*, 514. [CrossRef]